

Response to reviewer #1

We thank the reviewer for his/her evaluation of our paper and useful comments that helped improve the manuscript. We appreciate reviewer's time and effort in reviewing the manuscript. Below are responses to each comment. All reviewer's comments are in the standard font while the responses are in the italic font.

On behalf of the authors, Alexander Vasilkov

General comments:

1, The explicit aerosol corrections are only applied to the clear-sky part of a pixel, which causes inconsistency between the cloud and NO₂ retrieval.

We do not think that there is inconsistency between the cloud and NO₂ retrieval. Both cloud and NO₂ algorithms make use of the MLER model based on the independent pixel approximation with the same treatment of surface BRDF and aerosol in the clear-sky part of a pixel. The cloudy-sky part of a pixel is treated in the same manner as an opaque Lambertian surface with the same reflectivity of a commonly-accepted value of 80%. The basic assumption here is that aerosol is affecting the clear-sky part of the pixel only and is negligible in the cloudy part of the pixel. This assumption would fail for absorbing aerosol present above a cloud layer as discussed in the response to the next comment.

The studies of Lin et al., (2014) and Liu et al., (2019) have already shown the impacts of aerosols on cloud retrievals. Jethva et al., (2016) also showed absorbing aerosols were observed over clouds in spring and winter in Eastern China. So at least, the authors should discuss the impacts of explicit aerosol treatments on cloudy-sky retrievals.

It should be noted that NO₂ retrievals for cloudy sky conditions are highly uncertain and uncertainty can reach up to 100% (Boersma et al., 2011, Bucsela et al., 2013). Therefore, we recommend using NO₂ retrievals for clear and partially cloudy conditions only. Our focus here is on retrievals for low effective cloud fractions only, typically less than 0.25. We think that non-absorbing aerosol above the cloud with high reflectivity can be neglected. However, we agree that the impact of absorbing aerosol above the cloud is important and should be discussed.

We added the following in Sect. 2.5.1:

“It should be noted that a contribution of non-absorbing aerosol above a cloud with high reflectivity, as we assume within the MLER concept, to the cloud radiance is negligible. However, absorbing aerosol above the cloud can affect the cloud radiance. Analysis of frequency of occurrence of absorbing aerosol above the cloud derived from the 12-year record (2005–2016) of OMI led to the identification of regions with frequent aerosol–cloud overlap (Jethva et al., 2018). Figure 5 of that work showed that the most frequent aerosol–cloud overlap occurs over the oceans where the long-range transport of aerosols plays an important role and low-level marine stratocumulus clouds are observed. This fact is also confirmed in a recent paper by Zhang et al. (2019). Those oceanic regions are of less interest for tropospheric NO₂

retrievals because of the small contribution of anthropogenic NO₂ pollution. Additionally, tropospheric NO₂ retrievals over the oceanic regions are prone to errors from other aspects of retrievals (e.g., separation of stratospheric and tropospheric components), which are more important than aerosol effects. The springtime biomass burning activities such as burning of forest, grassland and crop residue over Southeast Asia release significant amounts of smoke particles observed over the widespread cloud deck over southern China on about 20%–40% of the cloudy days. NO₂ retrievals are typically not performed for those events owing to high cloud fractions. It is possible to flag and discard such retrievals if they were to occur in partial or thin cloud conditions using the absorbing aerosol index (Jethva et al., 2018). The treatment of absorbing aerosol over the cloud for NO₂ retrieval in such scenarios is beyond the scope of this work.”

Jethva, H., Torres, O., Ahn, C. A 12-year long global record of optical depth of absorbing aerosols above the clouds derived from the OMI/OMACA algorithm. *Atmos. Meas. Tech.*, 11, 5837–5864, 2018.

Zhang, W., Deng, S., Luo, T., Wu, Y., Liu, N., Li, X., Huang, Y. and Zhu, W.: New global view of above-cloud absorbing aerosol distribution based on CALIPSO measurements, *Remote Sens.*, 11, 2396; doi:10.3390/rs11202396, 2019.

2, The authors have listed plenty of comparisons in the introduction to illustrate the difference between satellite retrievals and other measurements. However, only one case study without any comparisons with ground- or aircraft-based data are discussed in the paper. The reviewer is doubt about the applicability of this method.

There is no doubt that explicit aerosol correction will reduce OMI low bias compared with ground-based data documented in numerous previous publications. Figure 9 compares current operational (b) and future (c) OMI tropospheric NO₂ retrievals. It shows that explicit aerosol correction enhances tropospheric NO₂ VCDs for all OMI pixels, which goes in right direction to mitigate general low bias in satellite NO₂ retrievals.

The authors should collect some measurements and make further comparisons since it seems that the method can be applied to anywhere globally. At least, more cases should be collected to reach comprehensive/valid analysis

Extensive OMI NO₂ comparisons with ground-based and aircraft measurements have been recently documented by our group (e.g. Choi et al., AMT, 2019) as well as other groups. Consensus has been reached that all current satellite tropospheric NO₂ measurements (OMI/GOME-2/TROPOMI) have low bias for highly polluted environments (Herman et al., AMT, 2019). Additional new comparisons are beyond the scope of this paper and are subject of a separate paper by our group (Lamsal et al., 2020, in preparation).

What this paper demonstrates, is that aerosol related uncertainties of current OMI (and for that matter TROPOMI) operational cloud (version 2.0) and tropospheric NO₂ (version 4.0) products can be unacceptably large under certain polluted conditions (e.g., Figs. 8-10), which certainly justifies consideration for implementation in the next version. Before operational

implementation, more rigorous comparison with a large collection of available ground-based data will be conducted.

Indeed, since we have already implemented GLER surface reflectance (which, by itself is explicitly aerosol corrected) in the current OMI operational algorithms, the next necessary step will be implementing explicit aerosol treatment in both cloud and NO₂ retrievals to make them consistent. Thus, the explicit aerosol correction is not only physically based, but indeed required for self-consistency of both cloud and NO₂ retrievals, which is necessary logical step prior to comparisons with ground-based and aircraft data.

Specific comments:

1, Line 3: “over norththeast Asia” should be “over northeastern Asia”. Based on the context, the authors only discussed a specific case over northeastern China.

Corrected.

2, Line 17: “top down” should be “top-down”. “assimilation” should be “assimilations”

Corrected.

3, Line 26: “optical properties” would be more accurate than “scattering properties”

Agree and done.

4, Line 27: Please cite (Castellanos et al., 2014; Liu et al., 2019)

Added.

5, Line 31: What do you mean by “detailed”?

We mean “modeling that includes treatment of clouds, the surface, and aerosols” as it is stated in the sentence.

6, Line 33: I do not think the definition of the Jacobians (AK) is the same as AMF.

Agree. We clarified this by replacing “or” by “needed for calculation of”.

7, Line 47: “southeast Asia” should be “Eastern China”

Corrected.

8, Line 48: “using data from the GEOS-Chem model with further adjustment through MODIS monthly AOD dataset.”

Added.

9, Line 51: Not exactly. Lin et al., (2014, 2015) and Liu et al., (2019) claimed that they used parallel RTM to ensure the efficiency of the calculation.

We mean that even with parallel RTM computations the cited studies were not carried out on a global scale as needed in operational processing of satellite instrument data. That is why we state that “these studies were carried out on a regional scale” in this sentence.

10, Line 175-180: See the general comment 1. Please add some specific case to help valid the argument here. “part of pixel only” should be “part of a pixel only”

We added some discussion here (see the answer to general comment #1). The missed article is added.

11, Line 244: What causes such an enhancement? It happens in this specific case or it related to the way that GEOS-5 uses to separate the troposphere and stratosphere?

This relatively small aerosol enhancement at altitudes of 11 km is thought to happen in this specific case. An exact cause of the enhancement is not clear.

12, Based on my understanding, the procedure for deriving GLER does not include aerosol optical properties, either. GLER is an important concept in this paper. Please add the definition or give a brief introduction to it.

You are right, GLER does not include aerosol contribution. It is calculated using atmospherically corrected BRDF data. We stated this in Sect. 2.4. We agree that adding the definition of GLER will be helpful. We added the definition and corresponding equation in Sect. 2.4. Lines 144-146 read now:

“The GLER is derived from TOA radiance computed for Rayleigh scattering and full surface BRDF for the particular geometry of a satellite instrument pixel. The TOA radiance computed by VLIDORT is then inverted to derive GLER using the following exact equation:

$$I_{TOA} = I_0 + GLER * T / (1 - GLER * S_b),$$

where I_0 is the TOA radiance calculated for a black surface, T is the total (direct+diffuse) solar irradiance reaching the surface converted to the ideal Lambertian-reflected radiance (by dividing by π) and then multiplied by the transmittance of the reflected radiation between the surface and TOA in the direction of a satellite instrument, and S_b is the diffuse flux reflectivity of the atmosphere for the case of its isotropic illumination from below (Vasilkov et al., 2017). All quantities, I_0 , T , and S_b are calculated using a known surface pressure for a given OMI pixel. The GLER concept has been evaluated with OMI over both land (Qin et al., 2019) and ocean (Fasnacht et al., 2019).”

Response to reviewer #3

We thank the reviewer for the evaluation of our paper and useful comments that helped improve the manuscript. We appreciate the reviewer's time and effort in reviewing the manuscript. Below are responses to each comment. All reviewer's comments are in the standard font while the responses are in the italic font.

On behalf of the authors, Alexander Vasilkov

Main comments

The method that is presented for the aerosol correction seems highly similar to the method presented by Lin et al (2014). Therefore, the claim that is made in the conclusions that this is new approach is not correct. It is a minor step forward compared to previously published work.

We agree that the method is similar to that presented by Lin et al. (2014) and we state this in Introduction Lines 71-72. However, there are two significant differences. First, it was necessary for Lin et al. (2014) to perform a lot of ad-hoc scaling of their GCM simulation results to match local aerosol observations in order to get realistic aerosol distributions. On the other hand, we are using a global assimilated aerosol product. One of the strengths of using the assimilated aerosol product is that this is generated by the assimilation system on a global scale in a seamless, consistent manner. One other important thing to note is that the GEOS aerosol assimilation product is constrained by MODIS and AERONET AOD observations at 550 nm. This is what differentiates our paper from Lin et al. (2014), and it is this consideration that allows for a global rather than regional methodology. Second, the method by Lin et al. (2014) is applicable to land surfaces only. We have developed a new treatment of surface BRDF for the ocean (Vasilkov et al., 2017). This approach for water surfaces is based on the GLER concept and has been validated in Fasnacht et al. (2019) and allows for a global processing of satellite instrument data.

We have rewritten Lines 73-75 and added the following text in Introduction:

“However, there are some significant differences. For instance, Lin et al. (2014) applied ad-hoc scaling of their global circulation model (GCM) simulation results to match local aerosol observations in order to get realistic aerosol distributions. On the other hand, we use an assimilated aerosol product (Buchard et al., 2017). One of the strengths of using the assimilated aerosol product is that it is processed on a global scale in a seamless, consistent manner. This allows for a global rather than a regional methodology as was the case in Lin et al. (2014) and Liu et al. (2020). The assimilated aerosol product provides a complete set of aerosol optical properties which include the vertically resolved aerosol layer optical depth, single scattering albedo, and phase scattering matrix computed for a given time and space location. Furthermore, the method by Lin et al. (2014) and Liu et al. (2020) is applicable to land surfaces only. We have developed a new treatment of surface BRDF for the ocean (Vasilkov et al., 2017). This approach for water surfaces has been validated in Fasnacht et al. (2019) and allows for a global and consistent processing of satellite NO₂ data.”

Although the authors claim that the method can be applied globally, there are computational problems to be resolved (line 312-319). The current description of the method is therefore incomplete for its global purpose. I believe it would be better to postpone publications until these problems are solved and a complete description can be given.

The one case that is presented is far too limited. Given that the authors claim to present a globally applicable method, global results for representative time periods need to be presented (e.g a few months). It is impossible to base any conclusions on the one case study that is presented.

The main objective of this study is to lay out and demonstrate the end to end approach of an explicit aerosol correction for a case study in a polluted region for an approach that is ultimately intended for global application. However, we do not initially intend to demonstrate the aerosol correction applicability on the global scale, as it is beyond the scope of this initial feasibility study. We intended to analyze global NO₂ retrievals in the second part of this study. Based on reviewer's suggestion, we processed OMI cloud and NO₂ data globally for the same day of April 5, 2005 as in the manuscript. It appears that the aerosol effect on spatial distribution of NO₂ retrievals is even more complex than expected from the previous model study and existing literature. It is well known that the main aerosol effect on NO₂ retrievals depends on relative vertical profiles of NO₂ and aerosol as well as aerosol optical properties. For clear skies, the aerosol can both increase and decrease sensitivity of satellite instrument measurements to tropospheric NO₂. Of course, the magnitude of this effect depends on aerosol optical depth (AOD) and single scattering albedo and to lesser extent on the phase scattering matrix. For partly cloudy scenes, the presence of aerosol affects both the cloud radiance fraction (CRF) and cloud pressure, a.k.a. cloud optical centroid pressure (OCP). CRF mostly decreases but OCP can both decrease and increase and its retrieval is impacted by the derived CRF. Processing OMI data on an orbital basis reveals additional and complex features of the aerosol effects ultimately on NO₂. We think that the full explanations of the aerosol effects on cloud and NO₂ retrievals could be a topic of a second part of this study.

Accounting for all those considerations we have reworded Lines 284-286 as follows:

“The application of our approach of the explicit aerosol correction to the selected area shows that the NO₂ increase due to the correction is in the right direction of reducing the documented low biases in the NO₂ retrievals with respect to ground- and aircraft-based observations.”

and added to the conclusions the following text:

“It should be noted that the above estimates of the explicit aerosol correction effects on cloud and NO₂ retrievals are valid for the selected area. More detailed investigation of the aerosol effects on the global scale will be carried out in the future work”.

As described in the literature and section 3.1, the aerosol effect depends on both the aerosol vertical profile and the NO₂ vertical profile. Whereas it is clear that the work uses Merra-2 profiles for the aerosols, it is not clear where the NO₂ profiles are coming from. This should be

described clearly, and in case there are not coming from Merra -2, it should be made clear why not.

NO₂ profiles and other model-derived information used in the computations are taken from the Global Modeling Initiative (GMI) model. The GMI simulation is driven by the meteorological fields from the MERRA-2. This is clarified in the revised manuscript as follows:

“NO₂ profiles and other model-derived information (e.g., temperature profiles, tropopause pressure) used in the computations are taken from the Global Modeling Initiative (GMI) model. The GMI simulation is driven by the meteorological fields from the MERRA-2. We use the GMI model because the simulations have been run consistently from the start of the OMI mission and this allows us to reprocess results from the entire OMI mission with the proposed aerosol correction.”

The fact that this method brings even more model information into the satellite retrievals is a concern. How can a user judge how much of the final retrieval product is model and how much is based on the measurements? This should be addressed in detail. Related to this, current NO₂ retrievals include averaging kernel information which allow users to replace the assumed NO₂ profile with their own profiles. It is preferable if a similar approach is implemented for the assumed aerosol profiles. This should also be addressed in the manuscript.

We do not agree with the reviewer’s characterization of our approach. MERRA-2 includes assimilation of aerosol optical depth from various ground and space-based remote sensing platforms. Our motivation for using aerosol information from MERRA-2 instead of a chemical transport model (e.g., GEOS-Chem) was to include observationally constrained data which takes advantage of the relative strengths of a model and observations.

The NASA NO₂ standard product does not include averaging kernel, but rather it includes scattering weight (SW) profiles and tropospheric and stratospheric AMFs that allow users to re-calculate the averaging kernels and VCDs using their own a-priori NO₂ profiles. This is possible because SWs are independent of a-priori NO₂ profiles. The new SWs accounting for aerosol profiles and surface BRDF will be provided in the new NO₂ product. The users can use the new SWs to correct for their custom NO₂ profiles. However, using a different aerosol profile and surface BRDF would require re-calculating SWs. It is an inherent issue with any explicit aerosol correction approach. We believe that our approach represents a reasonable compromise, which is feasible for global processing.

The sophistication of the aerosol and the cloud model seems to be out of balance. Whereas for the aerosol model a state-of-the-art aerosol model is applied, clouds are represented by a simple Lambertian clouds. The choice of this cloud model should be substantiated. Note that the retrieval results be as good as the weakest link in the chain.

For trace-gas retrievals it is important to estimate photon path lengths in the atmosphere that determine trace-gas absorption and thus affect the measured TOA radiances. Photon path lengths in a cloudy atmosphere are determined by the following most important cloud

parameters: the geometrical cloud fraction, the cloud optical depth, and the cloud vertical extent. Because of limited cloud informational content in TOA radiances, these three parameters cannot be retrieved simultaneously from the radiance measurements. That is why it is necessary to take on additional cloud assumptions. For instance, if a model of the Mie scattering cloud layer is used (Loyola et al., AMT, 2018), there is a need to assume a priori values for the cloud microphysical parameters and cloud vertical extent, to assume a homogeneous cloud layer and to add information about the cloud fraction from other measurements. We use a simpler model, the so-called mixed Lambertian-equivalent reflectivity (MLER) model that combines the independent pixel approximation and the treatment of cloud and ground as horizontally homogeneous, opaque Lambertian surfaces (Koelemeijer et al., JGR, 2001). The MLER model compensates for photon transport within a cloud by placing the equivalent Lambertian surface somewhere in the middle of the cloud instead of at the top (Stammes et al., JGR, 2008; Vasilkov et al., JGR, 2008; Sneep et al., JGR, 2008). As clouds are vertically inhomogeneous, the pressure of this surface does not necessarily correspond to the geometrical center of the cloud, but rather to the so called optical centroid pressure (OCP) (Joiner et al., AMT, 2012). The cloud OCP can be thought of and modeled as a reflectance-averaged pressure level reached by backscattered photons. The cloud OCP is the appropriate quantity for use in trace-gas retrievals from satellite instruments. Cloud-top pressures, e.g. those derived from thermal infrared measurements, are not equivalent to OCPs and do not provide good estimates of the required solar photon path lengths through clouds that are needed for trace-gas retrievals from UV-vis backscatter measurements (Vasilkov et al., JGR, 2008; Joiner et al., AMT, 2012). It has been demonstrated that the MLER model works reasonably well for trace-gas and cloud algorithms (Koelemeijer et al., JGR, 2001; Veeffkind et al., IEEE T. Geosci. Remote, 2006; Stammes et al., JGR, 2008; Boersma et al., AMT, 2011; Bucsela et al., AMT, 2013; Veeffkind et al., AMT, 2016).

Detailed comments

Section 2.5.1 This section should also describe cases for which the a-priori information is inconsistent with the measurements. For example, the following cases may occur: -The ECF becomes less than zero; -The ECF becomes larger than one; -The ECF is zero, but the SCD for O₂-O₂ is not consistent with aerosol profile. These are important details and all known geophysical situations should be covered in an algorithm paper.

We added the following text at the end of Section 2.5.1:

For a very small fraction of the ECF retrievals, ECF values can be outside the physically meaningful range of zero to one. We keep all the ECF retrievals in output orbital files thus providing the necessary diagnostic information on these physically unreasonable cases. Additionally we provide the clipped ECF retrievals, that is negative retrieved ECF values are replaced with zero and ECF values greater than one are replaced with one. Similarly, we provide these clipped CRF values as the input for the OMI NO₂ algorithm. A small fraction of the cloud OCP retrievals can also appear to be unphysical (values greater than surface pressure) (Veeffkind et al., 2016, Vasilkov et al., 2018). Again, we keep all OCP retrievals in output files and additionally provide clipped cloud OCP retrievals by replacing OCP values greater than the surface pressure with the actual surface pressure.

Section 2.5.1, line 183. Details shall be provided on how the equation is solved. What numerical methods are used?

We added the following at the end of Section 2.5.1:

To solve Eq. (4) we rewrite it in the form:

$$SCD_c(P_c) \equiv AMF_c(P_c) * VCD(P_c) = [SCD - AMF_g * VCD_g * (1 - f_r)] / f_r$$

where quantities on the right hand side of the equation are known, in particular, the quantity SCD is retrieved from the spectral fit of the OMI measurements around the O₂-O₂ absorption band at 477 nm (Vasilkov et al., 2018). Using LUT values of AMF_c(P_c) and calculated VCD(P_c) we then find the LUT pressure nodes P₁ and P₂ for which the following inequality is valid:

$$AMF_c(P_1) * VCD(P_1) < AMF_c(P_c) * VCD(P_c) < AMF_c(P_2) * VCD(P_2)$$

or equivalently,

$$SCD_1(P_1) < SCD_c(P_c) < SCD_2(P_2).$$

Then P_c can be obtained by linear interpolation of P over SCD:

$$P_c = [(SCD_c - SCD_1) * P_2 + (SCD_2 - SCD_c) * P_1] / (SCD_2 - SCD_1).$$

Section 2.2, line 121 How does Merra-2 deal with the very strongly non-linear growth of aerosol particles for relative humidities > 90%. This may be a frequently occurring at the top of the boundary layer for partly cloudy conditions and have significant effects on the AMF.

We agree that non-linear growth of aerosol particles can be important. However this topic is beyond the scope of our paper. Here we note that MERRA-2 does account for particle hygroscopic growth. Aerosol hygroscopic growth depends on simulated relative humidity and is considered in computations of particle fall velocity, deposition velocity, and optical parameters (Randles et al., 2017).

Section 2.3 Provide detailed information on the setup of the RT calculations wrt the aerosol optical properties, such as the number of streams used in calculations, etc.

In Section 2.3 we have added the following:

VLIDORT computes the single scattering contribution exactly in a spherically-curved atmosphere using the full scattering matrix. For multiple scattering, VLIDORT treats the direct solar beam attenuation in the pseudo-spherical approximation. This study used the delta-M scaling option to treat sharply peaked aerosol phase functions (Nakajima and Tanaka, 1988). We used 12 discrete ordinate streams in the polar hemisphere half space for the computation.

Nakajima, T., and M. Tanaka, Algorithms for radiative intensity calculations in moderately thick atmospheres using a truncation approximation. J. Quant. Spectrosc. Radiat. Transfer, 40, 51-69, 1988.

Section 3.2, line 249 The demonstrated effect is clearly not only because of BRDF effects. The largest effect is due to different source of the surface reflectivity data. If non BRDF effects were taken into account a similar effect could be expected.

This is true and it was discussed in Vasilkov et al. (2017). Here we have added the following:

“It should be noted that the differences include both BRDF effects and biases between the MODIS and OMI-based surface reflectance data sets. This is because the BRDF data and thus the GLERs are derived from atmospherically-corrected MODIS radiances while the climatological LERs are inherently affected by residual aerosols. Additionally, climatological LERs can be contaminated by clouds due to the substantially larger OMI pixel size as compared with MODIS footprints.”

Section 3.2 line 261 Also calibration differences between OMI and MODIS and atmospheric correction in MODIS should be discussed here.

We added the following:

“Calibration differences between OMI and MODIS are discussed in Qin et al. (2019) and specific details are provided in Appendix D: “Relative calibration of OMI and MODIS” of that paper. To summarize: MODIS Collection 5 radiances (used to derive BRDF kernel coefficients and thus GLER values) are higher than OMI Collection 3 radiances by approximately 1%. A sensitivity analysis of the equation used to compute GLER shows that a 1% error in TOA radiances will produce errors in LER of up to 0.003 in surface reflectivity. This value is much lower than the reported average difference between the climatological LER and GLER of 0.03. The atmospheric correction for MODIS band 3 used in this study has a theoretical error budget of about 0.005 reflectance units (Qin et al., 2019). Again, this error is much lower than the reported average difference suggesting that neither the calibration differences nor the MODIS atmospheric correction are major contributors to the observed difference between climatological LER and GLER.”

Section 3.2 line 298: “An interesting feature of the explicit aerosol correction on OCP is that the OCP can be reduced for a small fraction of the pixels.” This sentence is not understood.

We have reworded this sentence as follows: “An interesting effect of the explicit aerosol correction on OCP is that OCP values for high altitude clouds are lower for a few pixels within the selected area, while in general OCP are higher for the remaining bulk of pixels.”

Section 3.2 line 297: At low cloud fractions the errors in the OCP will explode. What is the assumed error in the OCPs? How does an increase of 50 hPa relate to the expected accuracy of the OCP?

That is correct. To clarify the issue we have added the following text:

“An OCP error is amplified with lower cloud fraction values. This is true all cloud pressure algorithms. In addition to OCP, we retrieve the so-called scene pressure (Vasilkov et al., 2018). In the absence of clouds and aerosols, the scene pressure should be equal to the surface pressure. A difference between the scene pressure and surface pressure can be considered as estimates of the OCP retrieval bias. This bias is about 40 hPa. Thus an increase of 50 hPa is comparable to the expected accuracy of the OCP retrievals. However, in our work we compare the OCP retrievals with and without the explicit aerosol correction. Even though these retrievals

possess bias, difference between them, e.g. increase of 50 hPa due to the implicit aerosol correction, does make sense.”

Explicit and consistent aerosol correction for visible wavelength satellite cloud and nitrogen dioxide retrievals based on optical properties from a global aerosol analysis

Alexander Vasilkov¹, Nickolay Krotkov², Eun-Su Yang¹, Lok Lamsal³, Joanna Joiner², Patricia Castellanos², Zachary Fasnacht¹, and Robert Spurr⁴

¹Science System and Applications, Inc., Lanham, MD, USA

²NASA Goddard Space Flight Center, Greenbelt, MD, USA

³Universities Space Research Association, Columbia, MD, USA

⁴RT Solutions, Inc., Cambridge, MA, USA

Correspondence: A. Vasilkov (alexander.vasilkov@ssaihq.com)

Abstract. We discuss an explicit and consistent aerosol correction for cloud and NO₂ retrievals that are based on the mixed Lambertian-equivalent reflectivity (MLER) concept. We apply the approach to data from the Ozone Monitoring Instrument (OMI) for a case study over ~~northeast Asian~~northeastern China. The cloud algorithm reports an effective cloud pressure, also known as cloud optical centroid pressure (OCP), from oxygen dimer (O₂–O₂) absorption at 477 nm after determining an effective cloud fraction (ECF) at 466 nm. The retrieved cloud products are then used as inputs to the standard OMI NO₂ algorithm. A geometry-dependent Lambertian-equivalent reflectivity (GLER), which is a proxy of surface bidirectional reflectance, is used for the ground reflectivity in our implementation of the MLER approach. The current standard OMI cloud and NO₂ algorithms implicitly account for aerosols by treating them as non-absorbing particulate scatters within the cloud retrieval. To explicitly account for aerosol effects, we use a model of aerosol optical properties from a global aerosol assimilation system and radiative transfer computations. This approach allows us to account for aerosols within the OMI cloud and NO₂ algorithms with relatively small changes. We compare the OMI cloud and NO₂ retrievals with implicit and explicit aerosol corrections over our study area.

1 Introduction

Global mapping of tropospheric trace-gas pollutants such as nitrogen dioxide (NO₂) and sulfur dioxide (SO₂) from ultraviolet (UV) and visible (Vis) spectrometers, such as the Ozone Monitoring Instrument (OMI) flying on the National Aeronautics and Space Administration (NASA) Aura satellite, has enabled many scientific studies and applications in air quality monitoring including “~~top-down~~top-down” emissions estimates, trend studies, and ~~assimilation~~assimilations into chemistry-transport models for “chemical weather” forecasts (see summary of Levelt et al., 2018). Recent progress has been facilitated by innovations in technology (i.e., satellite hyperspectral UV/Vis spectrometers with relatively high spatial resolution) as well as advances in trace-gas retrievals facilitated by development of linearized radiative transfer models (RTMs). While the trace-gas algorithms have matured greatly over the past few decades and have been scrutinized by comparisons with independent measurements

from ground- and aircraft-based [measurementsplatforms](#), there is still room for further improvement. For example, it has been long recognized that the effects of aerosols on trace-gas retrievals are significant, particularly in polluted regions, and affect both the trace gas retrieval itself as well as cloud retrievals that supply inputs to it (e.g., Martin et al., 2002; Boersma et al., 2004; Leitão et al., 2010; Castellanos et al., 2015; Lorente et al., 2017). Even for clear-sky conditions, aerosols impact trace gas retrievals in complicated ways due to different [scattering-optical](#) properties of various aerosol types and the relative vertical distributions of aerosols and gases ([e.g., Chimot et al., 2016](#))([e.g., Castellanos et al., 2015; Chimot et al., 2016; Liu et al., 2019](#)). While aerosol effects on cloud and trace-gas retrievals [themselves](#) have been known for some time, a globally consistent aerosol correction strategy has been hampered by two key obstacles: a lack of global distributions of aerosol optical property vertical profiles, and the need for accurate (on-line) and fast RTMs for both cloud and trace-gas retrievals that explicitly account for aerosol effects; existing RTMs tend to be computationally prohibitive in their native forms.

The retrieval of the vertical column density of a trace gas like NO₂ requires [a](#) detailed radiative transfer modeling that includes treatment of clouds, the surface, and aerosols. A linearized RTM is used to analytically calculate the Jacobians ~~or~~ [vertically-resolved-air-mass-factors](#)[needed for computation of vertically resolved Air Mass Factors](#), AMF(*h*), that are defined as sensitivities of satellite measured radiances with respect to a trace gas concentration at a given height *h*. While atmospheric molecular (Rayleigh) scattering limits satellite sensitivity to surface pollution, clouds and/or aerosols can either decrease (shielding effect) or enhance satellite sensitivity, depending on their optical properties and vertical distributions relative to the trace gas vertical profile (e.g., Palmer et al., 2001). Sensitivity studies suggest that weakly absorbing humidified aerosols typical of the eastern US in summer can cause NO₂ clear sky AMF to change by up to 8%; this is partially and implicitly accounted for in the cloud correction (Boersma et al., 2011). Lin et al. (2014, 2015) estimated much larger aerosol effects over eastern China (15-40% on annual mean NO₂ amounts) with large seasonal and regional [variabilityvariabilities](#).

Several studies have attempted to [explicitly](#) account for aerosol effects within limited regions. These studies have either used aerosol information from chemistry transport models (Martin et al., 2003; Lin et al., 2014, 2015), derived from the same instruments as used for the trace-gas retrievals (Chimot et al., 2019) and/or other instruments (Castellanos et al., 2015), or a combination of model and data retrieved from different instruments (Liu et al., 2019). In an analysis of the aerosol effects on NO₂ retrievals over South America during the biomass burning season, Castellanos et al. (2015) found 30-50% average differences in clear-sky NO₂ AMFs when aerosols were explicitly accounted for, but for individual pixels the AMFs could differ by more than a factor of two. Lin et al. (2014, 2015) reported better agreement with independent NO₂ observations over [southeast Asia-southeastern China](#) when aerosols are accounted for using data from the GEOS-Chem model [with further adjustment through MODIS monthly aerosol optical depth \(AOD\) dataset](#). Liu et al. (2019) further improved the aerosol correction for OMI tropospheric NO₂ retrievals over east Asia using constraints from Cloud-Aerosol Lidar with Orthogonal Polarization (CALIOP) aerosol vertical profiles. All of these studies were carried out on a regional scale owing to the high computational burden of on-line RT calculations needed to account for vertically-resolved aerosol effects within the NO₂ retrievals. Chimot et al. (2019) used ~~τ~~ -[AOD](#) and aerosol layer height derived from the O₂-O₂ absorption band on the same satellite instrument (Chimot et al., 2017, 2018) as inputs with a neural network based approach to derive this information in a computationally efficient manner. Recently, ~~Feit~~[JungJung et al. \(2019\)](#) suggested an explicit aerosol correction of the OMI

formaldehyde retrievals. They use aerosol information from the OMI UV aerosol algorithm, OMAERUV, and ~~lookup-look-up~~ tables of scattering weights to compute formaldehyde AMFs. Explicit aerosol effects on the cloud products are not accounted for.

60 Most of these studies focused on the effects of aerosol in clear sky retrievals. The effects of aerosol in the presence of overlaying cloud layers is important and Bousserez (2014) and Leitão et al. (2010) suggest that explicit account of aerosols in this case may improve NO₂ retrievals in such cases.

Cloud algorithms for UV/Vis sensors typically treat aerosols implicitly by providing effective (cloud + aerosol) cloud radiance fraction (CRF) and effective cloud pressure, a.k.a. cloud optical centroid pressure (OCP), both necessary inputs for
65 calculating AMF(*h*) in trace gas algorithms (e.g., Stammes et al., 2008). Thus, cloud effects on trace gas retrievals are compromised by the (unknown) aerosol effects and this may lead to errors in AMF(*h*). Surface reflectivity climatologies, based on data from the same instrument, may also erroneously incorporate the effects of aerosol, for example by being too bright in order to compensate for the presence of non-absorbing aerosol. These climatologies are used as inputs by both cloud and trace-gas algorithms and therefore may produce complex errors in AMF(*h*).

70 To explicitly account for aerosol effects on the OMI cloud and NO₂ retrievals, here we use three dimensional (3D) aerosol optical properties from a state-of-the-art global aerosol modeling and assimilation system and on-line RT calculations. We provide a demonstration of an envisioned global approach for a case study over a known polluted region of ~~southeast-Asian~~northeastern China. While the current approach is still computationally burdensome to apply globally, it is anticipated that faster versions of the RT code will be developed based on machine learning approaches.

75 In general, our approach to explicitly account for aerosol effects is similar to that used in Liu et al. (2019) and Lin et al. (2014, 2015). ~~A main difference is that we use a~~However, there are some significant differences. For instance, Lin et al. (2014) applied ad-hoc scaling of their global circulation model (GCM) simulation results to match local aerosol observations in order to get realistic aerosol distributions. On the other hand, we use an assimilated aerosol product (Buchard et al., 2017). One of the strengths of using the assimilated aerosol product is that it is processed on a global scale in a seamless, consistent manner. This allows for a global rather than a regional methodology as was the case in Lin et al. (2014) and Liu et al. (2019). The assimilated aerosol product provides a complete set of aerosol optical properties which include the vertically resolved aerosol layer optical depth, single scattering albedo, and phase scattering matrix computed for a given time and space location~~from the global aerosol modeling and assimilation system described in (Buchard et al., 2017).~~

. Furthermore, the method by Lin et al. (2014) and Liu et al. (2019) is applicable to land surfaces only. We have developed a new treatment of surface BRDF for the ocean (Vasilkov et al., 2017). This approach for water surfaces has been validated in Fasnacht et al. (2019) and allows for a global and consistent processing of satellite NO₂ data.

The main objective of this study is to lay out and demonstrate the end to end approach of an explicit aerosol correction and apply it to a case study in a polluted region for an approach that is ultimately intended for global application. We quantify the impact of such a correction in a polluted scenario. However, we do not validate our approach with independent ground- or
90 aircraft-based data as it is beyond the scope of this initial feasibility study.

The paper is structured as follows: Section 2 describes a general approach, assimilated aerosol parameters, surface reflectivity treatment, and the OMI cloud and NO₂ algorithms. Section 3 provides results and discussions of simulated aerosol effects on NO₂ AMFs for modeled aerosol profiles and a case study over a polluted region of northeast Asia. Conclusions and future work are described in Section 4.

95 2 Data and Methods

2.1 General framework for trace-gas retrievals from satellite UV/Vis spectrometers

Figure 1 shows a conceptual framework for trace gas retrievals from a satellite spectrometer (e.g., Aura OMI); this quantifies trace gas columns by analyzing spectral features in reflected sunlight. NO₂ and other gases like ozone O₃ and SO₂ each have their own unique spectral absorption signature. The differential optical absorption spectroscopy (DOAS) algorithm (Platt and
100 Stutz, 2008), converts these spectral signatures into a slant column density (SCD), the number of absorbing gas molecules along the effective photon path through the atmosphere to the satellite. The SCD is then converted into a vertical column density (VCD), the number of gas molecules in a vertical atmospheric column, using the concept of an air mass factor (AMF) that encapsulates the relationship between the measured SCD and VCD as $VCD = SCD/AMF$.

Theoretically, the relationship between SCD and VCD can be defined in terms of vertically resolved Jacobians, $J(h) =$
105 $-\partial \ln I / \partial \tau(h)$, where I is the top-of-atmosphere (TOA) radiance and $\tau(h)$ is the gaseous absorption optical thickness at altitude h . Generally, the AMF is calculated as

$$AMF = \int_0^{\infty} J(h)S(h)dh, \quad (1)$$

(Palmer et al., 2001) where $S(h)$ is the profile shape factor. For O₂–O₂, absorption is a function of the square of the pressure, and $S(h)$ is given by

$$110 \quad S(h) = \sigma(h)n^2(h) / \int_0^{\infty} \sigma(h)n^2(h)dh, \quad (2)$$

where $\sigma(h)$ is the O₂–O₂ absorption cross-section as a function of height ([because of its dependence of temperature](#)) and $n(h)$ is the number density of O₂.

Figure 2 shows an overall flow of our approach. The lower part of the diagram shows the trace-gas retrieval, in our case for NO₂ but this could apply to other trace-gases retrieved from UV/Vis sensors. Spectral fitting is applied to both O₂–O₂
115 for the subsequent cloud retrieval as well as to NO₂. Cloud parameters are then used as inputs to the NO₂ VCD algorithm. The other main inputs to the VCD algorithm are the clear- and cloud-sky Jacobians. For the Jacobian calculations, surface bidirectional reflectance distribution function (BRDF) parameters from the MODerate-resolution Imaging Spectroradiometer (MODIS) instruments are used as inputs along with the UV/Vis sensor (OMI) sun-satellite geometry as well as collocated aerosol optical properties. Details of the individual steps and input data are given below.

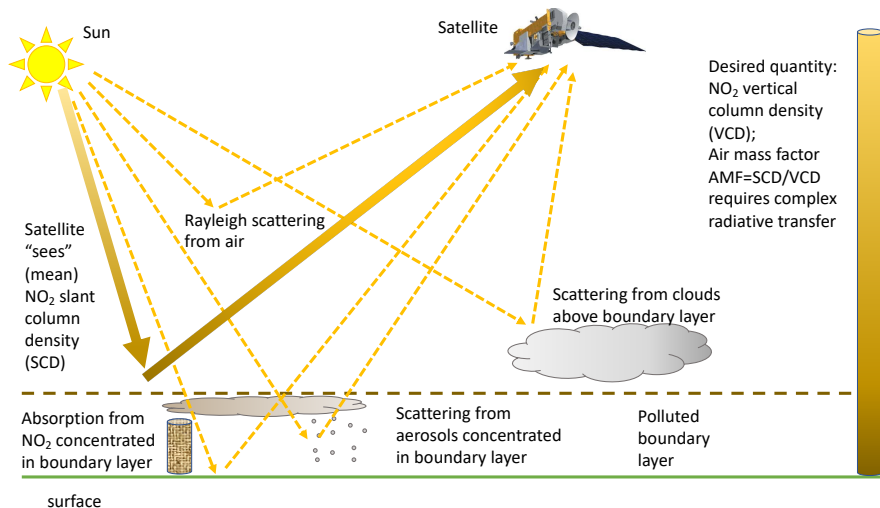


Figure 1. Conceptual diagram showing various paths of scattered and/or absorbed sunlight relevant to an NO₂ retrieval that may be observed from satellite along with standard terminology used for UV/Vis trace-gas retrievals.

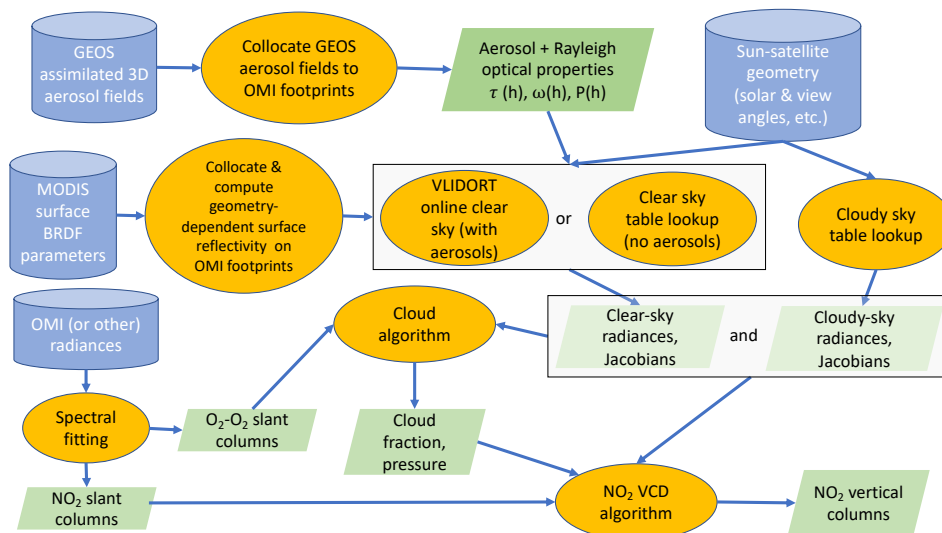


Figure 2. Flow diagram showing various steps and data used in our NO₂ retrievals.

120 2.2 Assimilated aerosol parameters

We use aerosol optical properties from the NASA Global Modeling and Assimilation Office (GMAO) Goddard Earth Observing System version 5 (GEOS-5) system (Randles et al., 2017). The GEOS-5 global aerosol data assimilation system incorporates

information from the MODIS and recently completed a multi-decadal aerosol reanalysis, the Modern-Era Retrospective Analysis for Research and Applications version 2 (MERRA-2) (Gelaro et al., 2017), that includes assimilation of the aerosol optical depth (AOD) from various ground- and space-based remote sensing platforms (Randles et al., 2017). The analysis system is driven by a prognostic model comprising the global atmospheric circulation model, GEOS-5, radiatively coupled to the Goddard Chemistry, Aerosol, Radiation, and Transport model (GOCART) (Colarco et al., 2010). The GOCART module simulates the production, loss, and transport of five types of aerosols (dust, sea salt, black carbon, organic carbon, and sulfate) treated as non-interactive external mixtures. The aerosol optical properties are described in Colarco et al. (2010) and are primarily based on the Optical Properties of Aerosols and Clouds database (Hess et al., 1998), with updates to dust properties to account for non-sphericity (Colarco et al., 2014).

The MERRA-2 global aerosol analysis data set provides vertically resolved 3D distributions of spectral aerosol layer optical depth, $\tau(h)$, single scattering albedo, $\omega_o(h)$, and scattering phase matrix, $P(h, \gamma)$ as a function of the scattering angle γ , on 72 layers from the surface to the top of the atmosphere at a native resolution of 0.5° latitude by 0.625° longitude [every 3 hours](#). These parameters are needed for the radiative transfer (RT) computations of TOA radiance and trace gas AMFs. The MERRA-2 aerosol analysis has been evaluated against independent (not assimilated) observations from ground-, aircraft-, space-, and ship-borne measurements ([\(Randles et al., 2017; Buchard et al., 2017\)](#) and [\(Randles et al., 2017; Buchard et al., 2017\)](#)). For instance, [comparisons of MERRA-2 analyzed AOD to historical \(1982-1996\) ship-borne measurements show that the model has a mean bias in AOD of 0.009, and a strong correlation with the observations \(\$r = 0.71\$ \), while a comparison to the Marine Aerosol Network \(MAN\) observations from 2004-2015 showed a mean bias of 0.01 and a standard error of 0.002 \(\$r = 0.93\$ \). MERRA-2 analyzed AOD was also compared to airborne High Spectral Resolution Lidar \(HSRL\) AOD observations during the Studies of Emissions and Atmospheric Composition, Clouds and Climate Coupling by Regional Surveys \(SEAC4RS\) campaign, which consisted of several flights during August-September 2013 over North America. Compared to HSRL observations, MERRA-2 AOD has a mean bias of 0.01, and standard error of 0.005 \(\$r = 0.85\$ \). The MERRA-2 aerosol analysis shows significant skill at representing dynamic global 3D aerosol distributions. For example, the MERRA-2 absorption aerosol optical depth \(AAOD\) and ultraviolet aerosol index \(AI\) compare well with OMI observations \(\[Buchard et al., 2017\]\(#\)\).](#)

2.3 RT calculations

For RT calculations here and elsewhere, we use the Vector Linearized Discrete Ordinate Radiative Transfer (VLIDORT) code (Spurr, 2006). VLIDORT computes the Stokes vector in a plane-parallel atmosphere with a Lambertian or non-Lambertian underlying surface. It has the ability to deal with attenuation of solar and line-of-sight paths in a spherical atmosphere, which is important for large solar zenith angles (SZA) and viewing zenith angles (VZA). This pseudo-spherical mode of VLIDORT was used in all our computations including on-line calculation and generation of lookup tables. [VLIDORT computes the single scattering contribution exactly in a spherically-curved atmosphere using the full scattering matrix. For multiple scattering, VLIDORT treats the direct solar beam attenuation in the pseudo-spherical approximation. This study used the delta-M scaling option to treat sharply peaked aerosol phase functions \(Nakajima and Tanaka, 1988\). We used 12 discrete ordinate streams in the polar hemisphere half space for the computation.](#)

2.4 Surface reflectivity treatment

The Earth's surface reflectance depends on illumination and observation geometry. The surface reflection anisotropy is described by the BRDF. To account for surface BRDF in our satellite algorithms, we have introduced the concept of a surface geometry-dependent LER (GLER) in Vasilkov et al. (2017). The GLER is derived from TOA radiance computed with-for Rayleigh scattering and full surface BRDF for the particular geometry of a satellite instrument pixel and-. The TOA radiance computed by VLIDORT is then inverted to derive GLER using the following exact equation:

$$I_{TOA} = I_0 + \frac{GLER * T}{1 - GLER * S_b}, \quad (3)$$

where I_0 is the TOA radiance calculated for a black surface, T is the total (direct+diffuse) solar irradiance reaching the surface converted to the ideal Lambertian-reflected radiance (by dividing by π) and then multiplied by the transmittance of the reflected radiation between the surface and TOA in the direction of a satellite instrument, and S_b is the diffuse flux reflectivity of the atmosphere for the case of its isotropic illumination from below (Vasilkov et al., 2017). All quantities, I_0 , T , and S_b are calculated using a known surface pressure for a given OMI pixel. The GLER concept has been evaluated with OMI over both land (Qin et al., 2019) and ocean (Fasnacht et al., 2019).

The GLER approach provides an exact match of TOA radiances with the full BRDF approach, i.e. the TOA radiance calculated with the full surface BRDF is equal to the radiance calculated with GLER. This approach does not require any major changes to existing MLER trace gas and cloud algorithms. It simply requires replacement of the static LER climatologies with GLERs pre-computed for a specific satellite instrument. We have incorporated GLERs based on a MODIS BRDF product and use these GLERs within OMI cloud and NO₂ algorithms (Vasilkov et al., 2017, 2018). It should be noted that Climatological LER values have inevitable cloud/aerosol contamination because they are derived from TOA radiance measurements by removing the Rayleigh scattering contribution only (Kleipool et al., 2008). The cloud/aerosol contribution is minimized by selecting lower values of the residuals, however it cannot be removed completely, partially due to relatively large OMI footprint. The OMI GLER is computed using the MODIS BRDF product, which is derived from the atmospherically corrected TOA reflectances (i.e., reflectance, that is after applying the MODIS cloud mask algorithm and removing aerosol scattering effects are removed at the high at the much higher spatial resolution of MODIS)-as compared with OMI. Therefore, the use of the GLER product in trace gas algorithms over heavily polluted regions greatly benefits from an explicit account of aerosols (Lin et al., 2015).

2.5 OMI data sets and algorithms

2.5.1 OMI cloud retrievals

The so-called mixed Lambert-equivalent reflectivity (MLER) concept is used in most OMI trace gas (Veefkind et al., 2006; Boersma et al., 2011; Krotkov et al., 2017) and cloud (Joiner and Vasilkov, 2006; Veefkind et al., 2016; Vasilkov et al., 2018) retrieval algorithms. It is also used in the TROPOMI NO₂ operational algorithm (Veefkind et al., 2012; van Geffen et al.,

2019) and in the Suomi-NPP OMPS formaldehyde algorithm (González Abad et al., 2016). The MLER model treats cloud and ground as horizontally homogeneous Lambertian surfaces and mixes them using the independent pixel approximation (IPA).
190 According to the IPA, the measured TOA radiance is a sum of the clear sky and overcast sub-pixel radiances that are weighted with an effective cloud fraction (ECF or f), i.e.,

$$I_m = I_g(R_g, \text{aer})(1 - f) + I_c(R_c) f, \quad (4)$$

where the aerosol optical properties, $\text{aer} = [\tau(h), \omega_0(h), P(h, \gamma)]$, are from the MERRA-2 global aerosol analysis. The ECF is calculated by inverting Eq. (4) at 466 nm, a wavelength little affected by gaseous absorption or rotational-Raman scattering.
195 The clear subpixel radiance, I_g , is computed on-line with the VLIDORT code for a given pixel geometry and surface pressure, P_s . The cloud radiance, I_c , is calculated using a pre-computed lookup table (LUT).

Our OMI cloud and NO_2 algorithms are based on the MLER model, ground and cloud being treated as Lambertian surfaces with pre-defined reflectivities. The ground reflectivity, R_g , is assumed to be represented by GLER that effectively accounts for surface BRDF (Vasilkov et al., 2017). The cloud reflectivity, R_c , is equal to 0.8 which is a common assumption (Stammes et al., 2008). Within the MLER model, here we explicitly account for aerosol for the clear-sky part of a pixel only. This is due to the simplifying treatment of cloud as an opaque surface, i.e. aerosol below the cloud does not contribute to the TOA radiance. Possible effects of aerosol above the cloud are neglected. Supporting arguments for this neglect are that aerosols are mostly observed within the planetary boundary layer, i.e. below clouds and [tropospheric](#) NO_2 retrievals are performed for low cloud fractions, usually for $\text{ECF} < 0.25$.

205 It should be noted that a contribution of non-absorbing aerosol above a cloud with high reflectivity, as we assume within the MLER concept, to the cloud radiance is negligible. However, absorbing aerosol above the cloud can decrease the cloud radiance. Analysis of frequency of occurrence of absorbing aerosol above the cloud derived from the 12-year record (2005–2016) of OMI led to the identification of regions with frequent aerosol–cloud overlap (Jethva and Torres, 2018). Figure 5 of that work showed that the most frequent aerosol–cloud overlap occurs over the oceans where the long-range transport of aerosols plays
210 an important role and low-level marine stratocumulus clouds are observed. This fact is also confirmed in a recent paper by Zhang et al. (2019). Those oceanic regions are of less interest for tropospheric NO_2 retrievals because of the small contribution of anthropogenic NO_2 pollution. Additionally, tropospheric NO_2 retrievals over the oceanic regions are sensitive to errors from other aspects of retrievals (e.g., separation of stratospheric and tropospheric components), which are more important than aerosol effects. The springtime biomass burning activities such as burning of forest, grassland and crop residue over Southeast
215 Asia release significant amounts of smoke particles observed over the widespread cloud deck over southern China on about 20–40% of the cloudy days. NO_2 retrievals are typically not performed for those events owing to high cloud fractions. It is possible to flag and discard such retrievals if they were to occur in partial or thin cloud conditions using the absorbing aerosol index (Jethva and Torres, 2018). The treatment of absorbing aerosol over the cloud for NO_2 retrieval in such scenarios is beyond the scope of this work.

220 Effective cloud pressure, also called the optical centroid pressure (OCP) (Joiner et al., 2012), is derived from the $\text{O}_2\text{--O}_2$ SCD calculated using spectral fitting of the absorption band at 477 nm. The OCP, here also denoted as P_c , is estimated using

the MLER method to compute the appropriate air mass factors (AMF) (Vasilkov et al., 2018). To solve for OCP, we invert the following equation

$$\text{SCD} = \text{AMF}_g(P_s, R_g, \text{aer}) \text{VCD}(P_s) (1 - f_r) + \text{AMF}_c(P_c, R_c) \text{VCD}(P_c) f_r, \quad (5)$$

225 where VCD is the vertical column density of O_2-O_2 ($\text{VCD} = \text{SCD} / \text{AMF}$), AMF_g and AMF_c are the precomputed (at 477 nm) clear sky (subscript g) and overcast (cloudy, subscript c) subpixel AMFs, P_s is the surface pressure, and f_r is the cloud radiance fraction (CRF) given by $f_r = f \times I_c / I_m$. CRF is defined as the fraction of TOA radiance reflected by the cloud. In Eq. (5) the CRF is calculated at 477 nm, the center of the O_2-O_2 absorption band. The O_2-O_2 absorption cross-section depends on height because we account for its temperature dependence (Thalman and Volkamer, 2013). The clear subpixel AMF, AMF_g , is
 230 computed on-line with the VLIDORT code while the cloudy subpixel AMF, AMF_c , is calculated using a pre-computed LUT.

To solve Eq. (5) we rewrite it in the form:

$$\text{SCD}_c(P_c) \equiv \text{AMF}_c(P_c) \text{VCD}(P_c) = [\text{SCD} - \text{AMF}_g \text{VCD}_g (1 - f_r)] / f_r, \quad (6)$$

where quantities on the right hand side of the equation are known, in particular, the quantity SCD is retrieved from the spectral fit of the OMI measurements around the O_2-O_2 absorption band at 477 nm (Vasilkov et al., 2018). Using LUT values of $\text{AMF}_c(P_c)$ and calculated $\text{VCD}(P_c)$ we then find the LUT pressure nodes P_1 and P_2 for which the following inequality is valid:

$$\text{AMF}_c(P_1) \text{VCD}(P_1) < \text{AMF}_c(P_c) \text{VCD}(P_c) < \text{AMF}_c(P_2) \text{VCD}(P_2) \quad (7)$$

or equivalently, $\text{SCD}_1(P_1) < \text{SCD}_c(P_c) < \text{SCD}_2(P_2)$. Then P_c can be obtained by linear interpolation of P over SCD:

$$240 \quad P_c = [(\text{SCD}_c - \text{SCD}_1) P_2 + (\text{SCD}_2 - \text{SCD}_c) P_1] / (\text{SCD}_2 - \text{SCD}_1). \quad (8)$$

For a very small fraction of the ECF retrievals, ECF values can be outside the physically meaningful range of zero to one. We keep all the ECF retrievals in output orbital files thus providing the necessary diagnostic information on these physically unreasonable cases. Additionally we provide the clipped ECF retrievals, that is negative retrieved ECF values are replaced with zero and ECF values greater than one are replaced with one. Similarly, we provide these clipped CRF values as the input for the OMI NO₂ algorithm. A small fraction of the cloud OCP retrievals can also appear to be unphysical (values greater than surface pressure) (Veefkind et al., 2016; Vasilkov et al., 2018). Again, we keep all OCP retrievals in output files and additionally provide clipped cloud OCP retrievals by replacing OCP values greater than the surface pressure with the actual surface pressure.

2.5.2 OMI NO₂ algorithm

250 The OMI NO₂ algorithm used here has a basis described in Krotkov et al. (2017) and references therein. Briefly, the NO₂ retrieval algorithm consists of determination of NO₂ SCD from a spectral fit of OMI-measured TOA radiance in the 402-465

nm window. The SCD is converted to VCD by using AMF calculated with various input parameters such as sun-viewing geometry, surface reflectivity, cloud pressure, cloud radiance fraction, and a priori NO₂ profile shapes. The characteristic vertical distribution of NO₂ and separation of the AMF into tropospheric and stratospheric components allow for nearly independent estimation of the respective VCDs. The NASA OMI NO₂-NO₂ algorithm used here utilizes a statistical approach, based on the OMI measurements, to estimate the stratospheric component (Bucsela et al., 2013).

Similar to the cloud algorithm, we explicitly account for aerosol in the calculation of tropospheric NO₂ clear-sky AMF only:

$$\text{AMF}_{\text{trop}} = \text{AMF}_g(P_s, R_g, \text{aer})(1 - f_r) + \text{AMF}_c(P_c, R_c)f_r, \quad (9)$$

In Eq. (9) the CRF is calculated at 440 nm, the center of the NO₂ fitting window. Calculation of clear sky AMF_g is carried out on-line using the VLIDORT code while calculation of cloud AMF_c is performed using a LUT.

3 Results and Discussion

3.1 Simulated aerosol effects on trace-gas AMFs

Aerosols can both increase and decrease sensitivity to trace gas absorption in satellite trace gas retrievals depending on their optical properties and vertical distributions relative to the trace gas vertical profile (Lin et al., 2014; Chimot et al., 2016). Aerosol scattering and absorption may shield photons from the atmosphere below, decreasing sensitivity to trace gas absorption. This effect is particularly pronounced when the primary layer of aerosols is located above the region of atmosphere that contains the trace gas of interest. Aerosol scattering within the trace gas layer increases photon path lengths and therefore may also enhance sensitivity to trace gas absorption.

To illustrate these effects, we conduct a theoretical study of the aerosol effects on NO₂ scattering weights for two model aerosol profiles. We perform calculations for a case where aerosols are elevated near the surface and another case where aerosols are present in an elevated layer (with a Gaussian shape and peak near 3 km altitude). For all computations, we use a single NO₂ profile that corresponds to a polluted region. For each aerosol profile we perform calculations for two values of ω_0 . We use $\omega_0 = 1.0$ for a case of non-absorbing aerosol and for the case of absorbing aerosols, we used $\omega_0 = 0.88$. For both cases we assumed that ω_0 is uniform throughout the atmosphere. For these computations, we set the surface albedo to 0.05, the VZA to zero (nadir), and the SZA to 45°. Based on the computed Jacobians, we calculate the NO₂ AMFs for the four different aerosol scenarios (two profiles and two values of ω_0).

Figure 3(left) shows the two model aerosol profiles along with a typical vertical profile of NO₂ number density for polluted areas. The total aerosol optical depth (AOD) for both aerosol profiles is equal to 1.0.

Figure 3(middle) compares the Jacobians with respect to NO₂ layer optical depth computed for non-absorbing aerosol profiles with the Jacobian for the aerosol-free atmosphere. Here, elevated aerosol clearly exhibits enhanced sensitivity to NO₂ above the aerosol layer and the shielding effect below. As a result of the shielding effect of the elevated aerosol, the values of NO₂ AMFs are lower than that for the aerosol-free NO₂ AMF. The near-surface aerosol enhances the sensitivity to NO₂

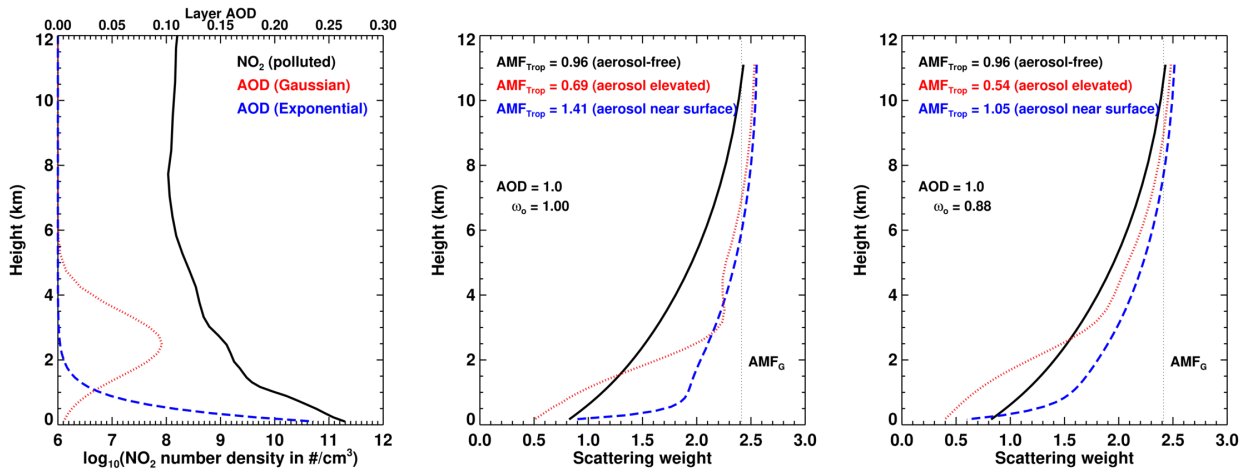


Figure 3. Left: Vertical profiles of tropospheric aerosols (layer aerosol optical depth (AOD), top scale) and the NO₂ number density (black lines, bottom scale). Middle: VLIDORT calculated NO₂ Jacobians for aerosol-free atmosphere (black lines) and mixed with non-absorbing (AOD=1.0, $\omega_0 = 1.0$) and absorbing (right: AOD=1.0, $\omega_0 = 0.88$) aerosols. The vertical dashed lines represent geometrical AMFs: $AMF = \sec(SZA) + \sec(VZA)$, where SZA and VZA are solar and view zenith angles. Right: Similar to the middle figure but for cases of absorbing aerosols (AOD=1.0, $\omega_0 = 0.88$).

almost for all altitudes; however, the enhanced sensitivity drops abruptly towards the surface owing to the increasing shielding effect.

Similarly, Figure 3(right) compares the Jacobians computed for absorbing aerosols with the Jacobian for the aerosol-free atmosphere. In general, aerosol absorption decreases the NO₂ sensitivity for both aerosol profiles. However, the qualitative dependence of the Jacobians on height remains similar to the nonabsorbing aerosol Jacobians.

3.2 Case study over northeast Asia

To demonstrate our explicit aerosol correction effects on the OMI cloud and NO₂ retrievals, we selected a cloud-free area over land in the Shenyang region of northeastern China. Figure 4 shows a map of OMI TOA reflectance over northeastern China calculated at 440 nm for orbit 3843 on April 5, 2005. The selected cloud-free area is shown by a square on this map. The GEOS-5 MERRA-2 aerosol optical properties were collocated over nominal OMI pixels within the area. There are total 114 OMI pixels within the selected area. The selected area has low cloud fractions (ECF<0.1), but significant aerosol loading, AOD ≈ 0.5 -0.6 according to the MERRA-2 data set.

Figure 5 shows vertical profiles of the layer AOD, SSA, and asymmetry parameter of a scattering phase function for different OMI pixels from the MERRA-2 data set within this selected area. The asymmetry parameter characterizes the anisotropy of the phase function, i.e. a size of aerosol particles. According to the MERRA-2 aerosol analysis, most aerosol is located in the

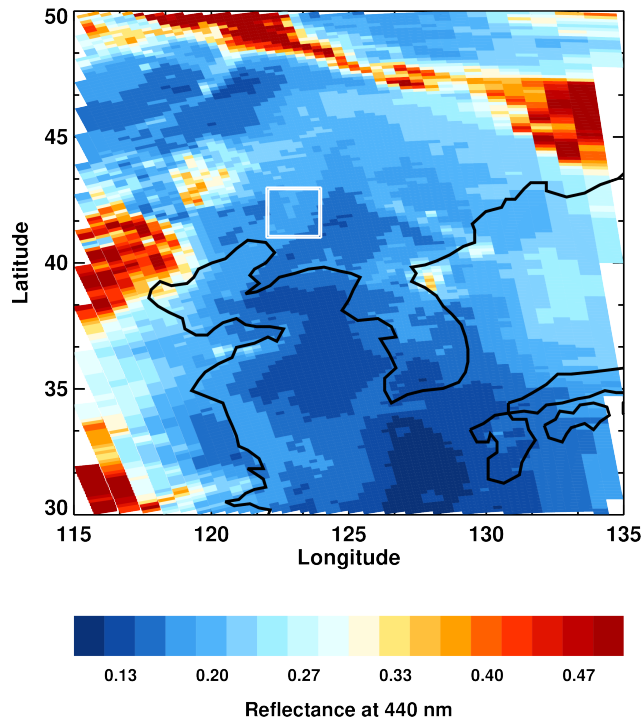


Figure 4. TOA reflectance at 440 nm over northeastern China for OMI orbit 3843 on 5 April 2005. The selected cloud-free region is denoted by a square.

planetary boundary layer (PBL) with significant increase in aerosol loading towards the surface. There is some enhancement
 300 of aerosol loading at altitudes of about 11 km. This aerosol plume at 11 km has distinctive optical properties with increased
 SSA (lower aerosol absorption) and increased asymmetry parameter (larger aerosol particles). The PBL aerosol has relatively
 low SSA within 0.83-0.88 and slightly increased asymmetry parameter (however lower than in the high altitude plume).

NO₂ profiles and other model-derived information (e.g., temperature profiles, tropopause pressure) used in the computations
 are taken from the Global Modeling Initiative (GMI) model. The GMI simulation is driven by the meteorological fields from
 the MERRA-2. We use the GMI model because the simulations have been run consistently from the start of the OMI mission
 and this allows us to reprocess results from the entire OMI mission with the proposed aerosol correction.
 305

Figure 6 shows both the climatological LER (Kleipool et al., 2008) and GLER for the selected area for OMI orbit 3843
 on April 5, 2005. We used the climatological LER for our cloud and NO₂ retrievals in the following figures for the purpose
 of demonstrating the BRDF effects on the retrievals. It is seen from Fig. 6 that values of GLER are noticeably lower than
 310 climatological LER values because the latter include inevitable aerosol contamination. On average, the difference between the
 climatological LER and GLER for this area is about 0.03. It should be noted that the differences include both BRDF effects and
 biases between the MODIS and OMI-based surface reflectance data sets. This is because the BRDF data and thus the GLERs
 are derived from atmospherically-corrected MODIS radiances while the climatological LERs are inherently affected by residual

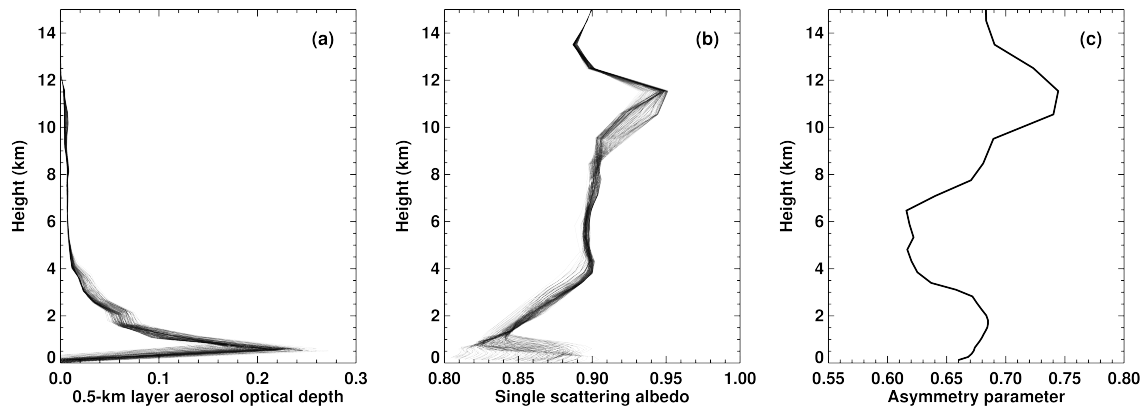


Figure 5. Vertical profiles of layer AOD (a), single scattering albedo (b), and asymmetry parameter (c) for different OMI pixels within the selected region.

315 aerosols. Additionally, climatological LERs can be contaminated by clouds due to the substantially larger OMI pixel size as compared with MODIS footprints. Calibration differences between OMI and MODIS are discussed in Qin et al. (2019) and specific details are provided in Appendix D: “Relative calibration of OMI and MODIS” of that paper. To summarize: MODIS Collection 5 radiances (used to derive BRDF kernel coefficients and thus GLER values) are higher than OMI Collection 3 radiances by approximately 1%. A sensitivity analysis of the equation used to compute GLER shows that a 1% error in TOA radiances will produce errors in LER of up to 0.003 in surface reflectivity. This value is much lower than the reported average difference between the climatological LER and GLER of 0.03. The atmospheric correction for MODIS band 3 used in this
 320 study has a theoretical error budget of about 0.005 reflectance units (Qin et al., 2019). Again, this error is much lower than the reported average difference suggesting that neither the calibration differences nor the MODIS atmospheric correction are major contributors to the observed difference between climatological LER and GLER.

Figure 7 compares ECF retrievals computed using climatological LERs with those computed using GLER and either implicit
 325 or explicit aerosol corrections. The comparison of ECFs retrieved with the climatological LER and the GLER and implicit aerosol correction shows the effects of replacing the surface climatological LER with the GLER only. As discussed earlier in Vasilkov et al. (2018), the GLERs are lower than the climatological LERs thus resulting in lower computed clear-sky radiances in Eq. (4) and subsequently higher retrieved ECFs. Explicit account of the aerosol contribution increases the computed clear-sky radiance thus reducing the retrieved ECF. The combined effect of GLER and explicit aerosol correction leads to ECFs
 330 slightly higher than those retrieved with the climatological LER for most pixels. The climatological LER is contaminated by aerosols and possibly clouds owing to substantially larger size of OMI pixels compared with those of MODIS data that are used for computation of GLER. That is why the lower ECFs retrieved with the climatological LER may indicate that the MERRA

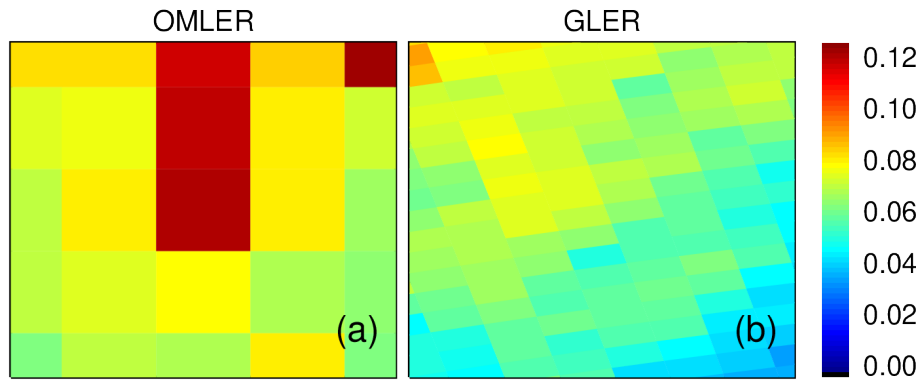


Figure 6. Surface LER at 440 nm over the selected area in the Shenyang region of northeastern China for OMI orbit 3843 on 5 April 2005; (a): monthly climatology at the original spatial resolution, (b): GLER computed for individual OMI pixels.

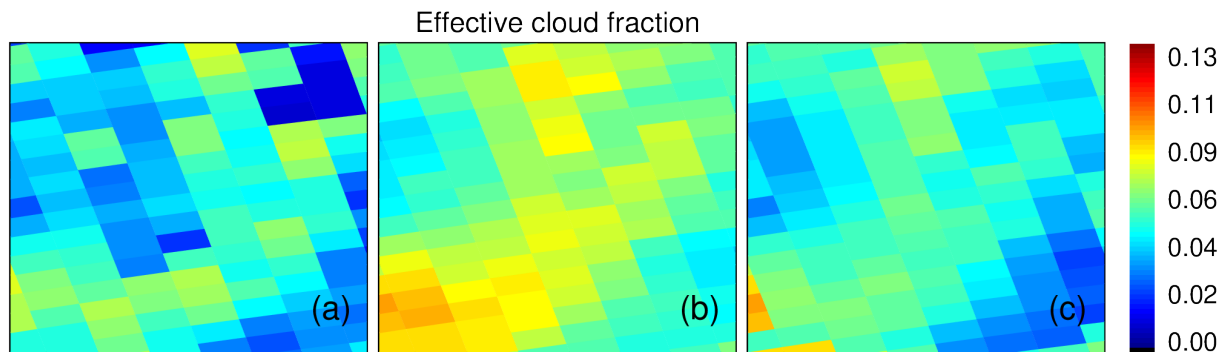


Figure 7. ECF retrieved with climatological surface LER (a), retrieved with GLER and implicit aerosol correction (b), and retrieved with GLER and explicit aerosol correction (c) over the selected area for OMI orbit 3843 on 5 April 2005.

AOD derived for this particular day is slightly lower than climatological AOD (and possibly residual cloud optical depth) for those pixels.

335 Similarly, Figure 8 compares OCP retrievals computed using the climatological LER with those calculated using the GLER and either implicit or explicit aerosol corrections. The GLER effect ~~only~~ on OCPs is mixed. For most OMI pixels, replacing the climatological LER with GLER results in lower OCPs. However for some pixels, this replacement leads to higher OCPs. It is not straightforward to explain the GLER effect on OCP because the retrieved OCP depends on both ECF and clear-sky O_2-O_2 AMF, both of which are affected by replacing the climatological LER with GLER. The comparison of OCPs retrieved
 340 with either implicit or explicit aerosol correction (Fig. 8b versus Fig. 8c) shows that the explicit aerosol correction significantly increases values of the OCPs for the overwhelming majority of OMI pixels. Again, this is a complex effect with multiple factors including the ECF calculation.

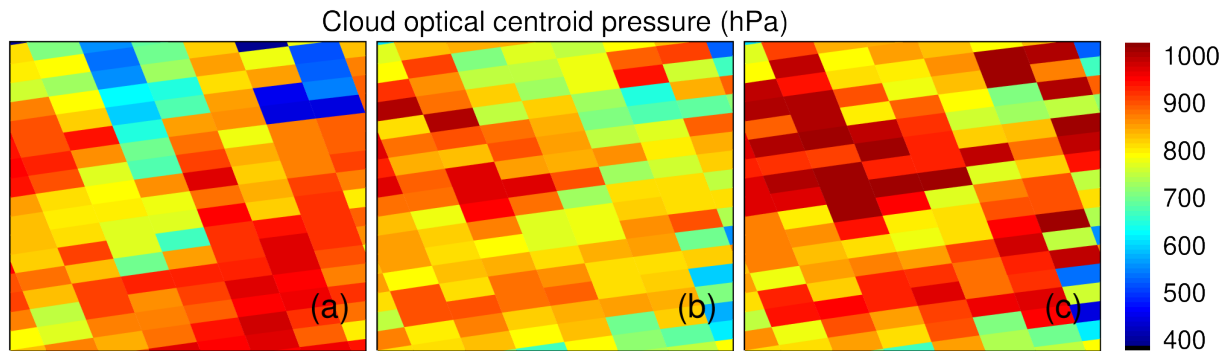


Figure 8. Similar to Fig. 7 but for cloud (optical centroid) pressure.

Finally, Figure 9 compares tropospheric NO₂ VCD retrievals computed using the climatological LER with those computed using the GLER and either implicit or explicit aerosol corrections. Replacing the climatological LER with GLER significantly increases the retrieved NO₂ amounts as has been shown previously for polluted areas in Vasilkov et al. (2017, 2018). The explicit aerosol correction additionally enhances the NO₂ vertical column density for all OMI pixels within the selected area. This enhancement is caused by the combined effect of the explicit aerosol correction on the cloud parameters and clear-sky NO₂ AMFs. This ~~is in the direction to account for documented~~ aerosol correction is in line with low biases in the satellite NO₂ retrievals as documented in several publications (Lamsal et al., 2014; Krotkov et al., 2017; Herman et al., 2019; Choi et al., 2019).

350 For instance, Herman et al. (2019) compared total NO₂ column retrievals from OMI with the ground-based Pandora at multiple sites in the US and South Korea, and found up to a factor of two lower column estimates by OMI. Assessment of OMI NO₂ retrievals with ground- and aircraft-based NO₂ observations during the DISCOVER-AQ (Deriving Information on Surface conditions from Column and Vertically Resolved Observations Relevant to Air Quality) and KORUS-AQ (Korea-United States Air Quality Study) field campaigns suggested that OMI NO₂ retrievals are about 20% lower as compared to validation

355 measurements even after accounting for the effect of a-priori NO₂ profiles and spatial mismatch using high-resolution NO₂ simulations (Choi et al., 2019). Both studies point to surface reflectivity and other factors in the NO₂ AMF for the low biases in OMI NO₂ retrievals. The application of our approach of the explicit aerosol correction to the selected area shows that the NO₂ increase due to the correction is in the direction of reducing the documented low biases in the OMI-NO₂ retrievals with respect to ground- and aircraft-based observations (Herman et al., 2019; Choi et al., 2019).

360 Given that the cloud fractions are very low for the selected area (ECF < 0.1), it is reasonable to suppose that the effect of the explicit aerosol correction on the NO₂ enhancement is mostly caused by decreasing the clear-sky AMF. The MERRA-2 aerosol data show absorbing aerosols for the selected area (see Fig. 5) particularly for near-surface aerosol. According to our RT simulations, the absorbing aerosols mostly decrease NO₂ AMFs for ~~polluted regions- this case~~. However, our preliminary analysis outside of the selected area reveals more complex picture demonstrating both shielding and enhancement aerosol

365 effects. A global analysis of the aerosol effects will be a subject of our follow-up paper.

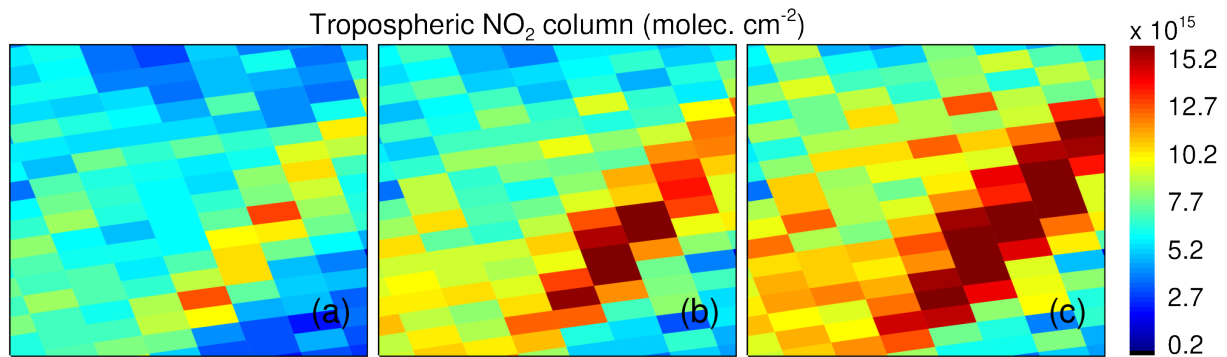


Figure 9. Similar to Fig. 7 but for tropospheric (trop.) NO₂ vertical column density.

Figure 10 further elucidates the effect of explicit aerosol correction on cloud and NO₂ retrievals. It shows scatter plots of ECF, OCP, and tropospheric NO₂ computed with GLER and implicit versus explicit aerosol corrections. The explicit aerosol correction consistently increases the retrieved ECF within the whole range of ECFs. This ECF increase does not depend on an ECF value and is equal to approximately 0.015 on average. OCP changes due to the explicit aerosol correction generally depend on the value of OCP. The OCP increases with explicit account of aerosol for the overwhelming majority of pixels. This OCP increase is most pronounced for high values of OCP, i.e. for low altitude clouds. For such clouds, the OCP increases by about 100 hPa. The OCP increase is approximately 50 hPa for mid-altitude clouds with OCP of about 800 hPa. **An interesting feature** ~~An interesting effect~~ of the explicit aerosol correction on OCP is that ~~the OCP can be reduced for a small fraction of the OCP values for high altitude clouds are lower for a few pixels within the selected area, while in general OCP are higher for the remaining bulk of pixels.~~ Particularly it is true for high altitude clouds with OCP values of about 500 hPa. It should be noted that an OCP error is amplified with lower cloud fraction values. This is true all cloud pressure algorithms. In addition to OCP, we retrieve the so-called scene pressure (Vasilkov et al., 2018). In the absence of clouds and aerosols, the scene pressure should be equal to the surface pressure. A difference between the scene pressure and surface pressure can be considered as estimates of the OCP retrieval bias. This bias is about 40 hPa. Thus an increase of 50 hPa is comparable to the expected accuracy of the OCP retrievals. However, in our work we compare the OCP retrievals with and without the explicit aerosol correction. Even though these retrievals possess bias, difference between them, e.g. increase of 50 hPa due to the implicit aerosol correction, does make sense.

The explicit aerosol correction increases the tropospheric NO₂ VCDs for all OMI pixels of the selected area by approximately 20% on average. This indicates that the aerosol shielding effect prevails over the effect of aerosol enhancement of photon path length for the selected area.

The uncertainties in tropospheric NO₂ retrievals arise from the uncertainties in NO₂ slant column retrievals, in the AMF calculations, and from the stratosphere-troposphere separation scheme. The uncertainty in NO₂ slant columns is about 0.8×10^{15} molec cm⁻², which is typically less than 7% in high slant column cases (either over polluted areas or for observations at high solar zenith angle) and reaches up to 20% in clean areas. Uncertainties in the AMF are 20-80%, and dominate

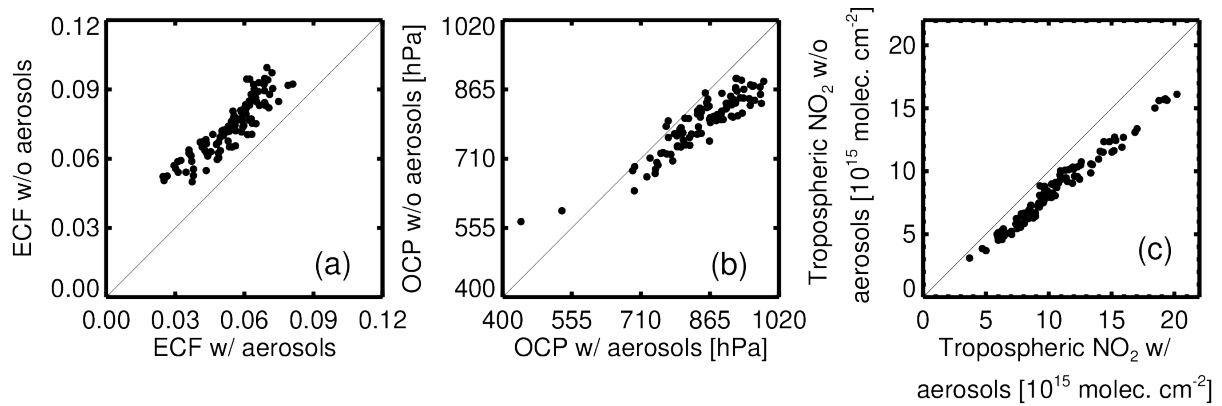


Figure 10. Scatter plots of retrieved quantities with implicit aerosol correction versus those retrieved with explicit aerosol correction for the selected area in OMI orbit 3843 on 5 April 2005. (a): Effective cloud fraction at 466 nm (ECF_{466}), (b): Cloud Optical Centroid Pressure (OCP), and (c): Tropospheric NO_2 vertical column density.

390 [the overall retrieval uncertainties \(Martin et al., 2002; Boersma et al., 2011; Bucsele et al., 2013; Lin et al., 2014\)](#) Errors in the
[a-priori vertical \$NO_2\$ profile shape, surface reflectivity, and cloud-aerosol treatment are the largest error sources \(Boersma et al., 2011; Lam](#)
[The uncertainty in the stratosphere-troposphere separation is expected to be less than \$0.3 \times 10^{15}\$ molec \$cm^{-2}\$, especially in](#)
[polluted areas \(Bucsele et al., 2013\). Consistent with prior studies by Lin et al. \(2014\) and Liu et al. \(2019\), our study suggests](#)
[that the aerosol effect over China is significant, and is similar to that of a-priori \$NO_2\$ profile shape and surface reflectivity.](#)

395 It should be noted that we used the vector VLIDORT code (Spurr, 2006) to calculate TOA radiances and vertically resolved
 O_2-O_2 and NO_2 Jacobians in our case study. Such calculations have been too computationally expensive for on-line use in
 global processing of multi-year satellite data records. A scalar approximation to the radiative transfer equation implemented
 using the LIDORT code is much faster than VLIDORT and save computational costs by about an order of magnitude. However
 the LIDORT produces errors in TOA radiance as large as 10% due to neglect of polarization effects. Recently, an artificial
 400 neural network (NN) technique to correct TOA radiances from the LIDORT to within 1% of vector-calculated radiances has
 been developed (Castellanos and da Silva, 2019). We plan to optimize the NN technique for the OMI cloud and NO_2 algorithms
 and extend it to calculate vertically-resolved Jacobians.

4 Conclusions

We discuss a new approach to explicitly account for aerosol effects on cloud and NO_2 retrievals. This approach can be easily
 405 incorporated into the existing [operational](#) algorithms based on the MLER concept. A main feature of the approach is that we use
 a complete set of aerosol optical properties which include the vertically resolved aerosol layer optical depth, single scattering
 albedo, and phase scattering matrix computed for a given time and space location from the global aerosol modeling and assim-
 ilation system. The surface BRDF is accounted for in the RT computations using the GLER concept (Vasilkov et al., 2017),

that provides a computationally efficient method of treating BRDF in the MLER-based satellite algorithms. Comparisons of
410 the new explicit with ~~the~~ existing implicit aerosol correction over a polluted case study area in northeast ~~Asia~~ ~~China~~ show that
our explicit aerosol correction over polluted areas (1) decreases the retrieved ECF by 0.015 on average; (2) increases the OCP
by about 100 hPa for low altitude clouds and about 50 hPa for mid-altitude clouds; and (3) increases the tropospheric NO₂
retrievals by about 20%. This NO₂ enhancement due to the explicit aerosol correction could reduce the documented biases
in the OMI NO₂ retrievals with respect to ground- and aircraft-based observations (Herman et al., 2019; Choi et al., 2019). It
415 should be noted that the above estimates of the explicit aerosol correction effects on cloud and NO₂ retrievals are valid for the
selected area. More detailed investigation of the aerosol effects on the global scale will be carried out in the future work.

Our approach requires on-line computations because it is difficult to implement a look-up table technique for inputs that
include vertically-resolved optical parameters of aerosol. Currently, the on-line VLIDORT computations are not feasible for
global processing of satellite data, particularly from high spatial resolution instruments such as TROPOMI and upcoming
420 geostationary missions such as Korean Geostationary Environment Monitoring Spectrometer (GEMS), the ~~US~~-NASA Tropo-
spheric Emissions: Monitoring of Pollution (TEMPO), and the European Space Agency (ESA) Sentinel 4. We plan to further
develop the NN technique (Castellanos and da Silva, 2019) to speed up the RT computations and apply our explicit aerosol
correction to operational processing of OMI data globally.

Future work will also include a more comprehensive implementation of this approach, particularly such that results may
425 be quantitatively compared with ground- and aircraft-based data collected during intensive field campaigns at a variety of
locations and under different meteorological and chemical scenarios.

Data availability. The MODIS gap-filled BRDF Collection 5 product MCD43GF used for calculation of GLER in this paper is available at
ftp://rsftp.eos.umb.edu/data02/Gapfilled/. The OMI Level 1 data used for calculations of GLER are available at
https://aura.gesdisc.eosdis.nasa.gov/data/Aura_OMI_Level1/. The OMI Level 2 Collection 3 data that include cloud, NO₂, and OMI pixel
430 corner products are available at https://aura.gesdisc.eosdis.nasa.gov/data/Aura_OMI_Level2/.

Author contributions. AV analyzed aerosol effects on the cloud and NO₂ retrievals and wrote the manuscript. NK developed the GLER
concept and participated in writing the manuscript. ESY performed computations of the O₂–O₂ and NO₂ scattering weights and retrievals
of cloud parameters. LL applied the GLER and cloud retrievals to the NO₂ retrieval algorithm. JJ developed the cloud OCP concept and
participated in writing the manuscript. PC calculated vertical profiles of aerosol optical properties. ZF provided collocation of GEOS-5
435 aerosol data onto OMI ground pixels. RS developed the VLIDORT code used for computation of the scattering weights.

Competing interests. The authors declare that they have no conflict of interest.

Acknowledgements. Funding for this work was provided by NASA through Aura core team funding as well as the Aura project and Aura Science Team and Atmospheric Composition Modeling and Analysis Program managed by Kenneth Jucks and Barry Lefer. This work was funded in part by the NO₂ MEaSUREs project led by L. ~~Lok~~[Lamsal](#), grant number 80NSSC18M0086.

440 References

- Boersma, K. F., Eskes, H. J., and Brinksma, E. J.: Error analysis for tropospheric NO₂ retrieval from space, *J. Geophys. Res.- Atmos.*, 109, <https://doi.org/10.1029/2003JD003962>, 2004.
- Boersma, K. F., Eskes, H. J., Dirksen, R. J., van der A, R. J., Veefkind, J. P., Stammes, P., Huijnen, V., Kleipool, Q. L., Sneep, M., Claas, J., Leitão, J., Richter, A., Zhou, Y., and Brunner, D.: An improved tropospheric NO₂ column retrieval algorithm for the Ozone Monitoring Instrument, *Atmos. Meas. Tech.*, 4, 1905–1928, <https://doi.org/10.5194/amt-4-1905-2011>, <https://www.atmos-meas-tech.net/4/1905/2011/>, 2011.
- 445 Bousseres, N.: Space-based retrieval of NO₂ over biomass burning regions: quantifying and reducing uncertainties, *Atmos. Meas. Tech.*, 7, 3431–3444, <https://doi.org/10.5194/amt-7-3431-2014>, 2014.
- Buchard, V., Randles, C. A., da Silva, A. M., Darmenov, A., Colarco, P. R., Govindaraju, R., Ferrare, R., Hair, J., Beyersdorf, A. J., Ziemba, L. D., and Yu, H.: The MERRA-2 aerosol reanalysis, 1980 onward. Part II: evaluation and case studies, *J. Clim.*, 30, 6851–6872, <https://doi.org/10.1175/JCLI-D-16-0613.1>, 2017.
- 450 Bucsela, E., Krotkov, N., Celarier, E., Lamsal, L., Swartz, W., Bhartia, P., Boersma, K., Veefkind, J., Gleason, J., and Pickering, K.: A new stratospheric and tropospheric NO₂ retrieval algorithm for nadir-viewing satellite instruments: applications to OMI, *Atmos. Meas. Tech.*, 6, 2607–2626, <https://doi.org/10.5194/amt-6-2607-2013>, 2013.
- 455 Castellanos, P. and da Silva, A.: A neural network correction to the scalar approximation in radiative transfer, *J. Atmos. Ocean. Tech.*, 36, 819–832, <https://doi.org/10.1175/JTECH-D-18-0003.1>, 2019.
- Castellanos, P., Boersma, K. F., Torres, O., and de Haan, J. F.: OMI tropospheric NO₂ air mass factors over South America: effects of biomass burning aerosols, *Atmos. Meas. Tech.*, 8, 3831–3849, <https://doi.org/10.5194/amt-8-3831-2015>, 2015.
- Chimot, J., Vlemmix, T., Veefkind, J. P., de Haan, J. F., and Levelt, P. F.: Impact of aerosols on the OMI tropospheric NO₂ retrievals over industrialized regions: how accurate is the aerosol correction of cloud-free scenes via a simple cloud model?, *Atmos. Meas. Tech.*, 9, 359–382, <https://doi.org/10.5194/amt-9-359-2016>, 2016.
- 460 Chimot, J., Veefkind, J. P., Vlemmix, T., de Haan, J. F., Amiridis, V., Proestakis, E., Marinou, E., and Levelt, P. F.: An exploratory study on the aerosol height retrieval from OMI measurements of the 477 nm O₂–O₂ spectral band using a neural network approach, *Atmos. Meas. Tech.*, 10, 783–809, <https://doi.org/10.5194/amt-10-783-2017>, 2017.
- 465 Chimot, J., Veefkind, J. P., Vlemmix, T., and Levelt, P. F.: Spatial distribution analysis of the OMI aerosol layer height: a pixel-by-pixel comparison to CALIOP observations, *Atmos. Meas. Tech.*, 11, 2257–2277, <https://doi.org/10.5194/amt-11-2257-2018>, 2018.
- Chimot, J., Veefkind, J. P., de Haan, J. F., Stammes, P., and Levelt, P. F.: Minimizing aerosol effects on the OMI tropospheric NO₂ retrieval – An improved use of the 477 nm O₂–O₂ band and an estimation of the aerosol correction uncertainty, *Atmos. Meas. Tech.*, 12, 491–516, <https://doi.org/10.5194/amt-12-491-2019>, 2019.
- 470 Choi, S., Lamsal, L. N., Follette-Cook, M., Joiner, J., Krotkov, N. A., Swartz, W. H., Pickering, K. E., Loughner, C. P., Appel, W., Pfister, G., Saide, P. E., Cohen, R. C., Weinheimer, A. J., and Herman, J. R.: Assessment of NO₂ observations during DISCOVER-AQ and KORUS-AQ field campaigns, *Atmos. Meas. Tech. Discuss.*, 12, 1–33, <https://doi.org/10.5194/amt-2019-338>, 2019.
- Colarco, P., da Silva, A., Chin, M., and Diehl, T.: Online simulations of global aerosol distributions in the NASA GEOS-4 model and comparisons to satellite and ground-based aerosol optical depth, *J. Geophys. Res. - Atmos.*, 115, <https://doi.org/10.1029/2009JD012820>, 2010.
- 475

- Colarco, P., Nowottnick, E., Yi, B., Yang, P., and Kim, K. e. a.: Impact of radiatively interactive dust aerosols in the NASA GEOS-5 climate model: Sensitivity to dust particle shape and refractive index, *Journal of Geophysical Research: Atmospheres*, 119, <https://doi.org/10.1029/2013JD020046>, 2014.
- 480 Fasnacht, Z., Vasilkov, A., Haffner, D., Qin, W., Joiner, J., Krotkov, N., Sayer, A. M., and Spurr, R.: A geometry-dependent surface Lambertian-equivalent reflectivity product for UV/Vis retrievals: Part II. Evaluation over open ocean, *Atmos. Meas. Tech. Discuss.*, 2019, 1–33, <https://doi.org/10.5194/amt-2019-260>, 2019.
- Gelaro, R., McCarty, W., Suárez, M. J., Todling, R., Molod, A., Takacs, L., Randles, C. A., Darmenov, A., Bosilovich, M. G., Reichle, R., Wargan, K., Coy, L., Cullather, R., Draper, C., Akella, S., Buchard, V., Conaty, A., da Silva, A. M., Gu, W., Kim, G.-K., Koster, R., Lucchesi, R., Merkova, D., Nielsen, J. E., Partyka, G., Pawson, S., Putman, W., Rienecker, M., Schubert, S. D., Sienkiewicz, M., 485 and Zhao, B.: The Modern-Era Retrospective Analysis for Research and Applications, version 2 (MERRA-2), *J. Clim.*, 30, 5419–5454, <https://doi.org/10.1175/JCLI-D-16-0758.1>, 2017.
- González Abad, G., Vasilkov, A., Seftor, C., Liu, X., and Chance, K.: Smithsonian Astrophysical Observatory Ozone Mapping and Profiler Suite (SAO OMPS) formaldehyde retrieval, *Atmos. Meas. Tech.*, 9, 2797–2812, <https://doi.org/10.5194/amt-9-2797-2016>, 2016.
- Herman, J., Abuhassan, N., Kim, J., Kim, J., Dubey, M., Raponi, M., and Tzortziou, M.: Underestimation of column NO₂ amounts from the 490 OMI satellite compared to diurnally varying ground-based retrievals from multiple PANDORA spectrometer instruments, *Atmos. Meas. Tech.*, 12, 5593–5612, <https://doi.org/10.5194/amt-12-5593-2019>, 2019.
- Hess, M., Koepke, P., and Schult, I.: Optical Properties of Aerosols and Clouds: The Software Package OPAC, *Bulletin of the American Meteorological Society*, 79, 831–844, 1998.
- Jethva, H. and Torres, O. and Ahn, C.: A 12-year long global record of optical depth of absorbing aerosols above the clouds derived from the 495 OMI/OMACA algorithm, *Atmos. Meas. Tech.*, 11, 5837–5864, 2018.
- Joiner, J. and Vasilkov, A. P.: First results from the OMI rotational Raman scattering cloud pressure algorithm, *IEEE Trans. Geos. Rem. Sens.*, 44, 1272–1282, <https://doi.org/10.1109/TGRS.2005.861385>, 2006.
- Joiner, J., Vasilkov, A. P., Gupta, P., Bhartia, P. K., Veeffkind, P., Sneep, M., de Haan, J., Polonsky, I., and Spurr, R.: Fast simulators for satellite cloud optical centroid pressure retrievals; evaluation of OMI cloud retrievals, *Atmos. Meas. Tech.*, 5, 529–545, 500 <https://doi.org/10.5194/amt-5-529-2012>, 2012.
- Jung, Y., Gonzalez Abad, G., Nowlan, C., Chance, K., Liu, X., Torres, O., and Ahn, C.: Explicit aerosol correction of OMI formaldehyde retrievals, *Earth Space Sci.*, 6, 1–19, <https://doi.org/10.1029/2019EA000702>, 2019.
- Kleipool, Q. L., Dobber, M. R., de Haan, J. F., and Levelt, P. F.: Earth surface reflectance climatology from 3 years of OMI data, *J. Geophys. Res. - Atmos.*, 113, <https://doi.org/10.1029/2008JD010290>, 2008.
- 505 Krotkov, N. A., Lamsal, L. N., Celarier, E. A., Swartz, W. H., Marchenko, S. V., Bucsela, E. J., Chan, K. L., Wenig, M., and Zara, M.: The version 3 OMI NO₂ standard product, *Atmos. Meas. Tech.*, 10, 3133–3149, <https://doi.org/10.5194/amt-10-3133-2017>, 2017.
- Lamsal, L. N., Krotkov, N. A., Celarier, E. A., Swartz, W. H., Pickering, K., Bucsela, E. J., Gleason, J., Martin, R., Philip, S., Irie, H., Cede, A., Herman, J., Weinheimer, A., Szykman, J., and Knepp, T.: Evaluation of OMI operational standard NO₂ column retrievals using in situ and surface-based NO₂ observations, *Atmos. Chem. Phys.*, 14, 11 587–11 609, <https://doi.org/10.5194/acp-14-11587-2014>, 2014.
- 510 Leitão, J., Richter, A., Vrekoussis, M., Kokhanovsky, A., Zhang, Q. J., Beekmann, M., and Burrows, J. P.: On the improvement of NO₂ satellite retrievals – aerosol impact on the air mass factors, *Atmos. Meas. Tech.*, 3, 475–493, <https://doi.org/10.5194/amt-3-475-2010>, 2010.

- Levelt, P. F., Joiner, J., Tamminen, J., Veefkind, J. P., Bhartia, P. K., Stein Zweers, D. C., Duncan, B. N., Streets, D. G., Eskes, H., van der A, R., McLinden, C., Fioletov, V., Carn, S., de Laat, J., DeLand, M., Marchenko, S., McPeters, R., Ziemke, J., Fu, D., Liu, X., Pickering, K., Apituley, A., González Abad, G., Arola, A., Boersma, F., Chan Miller, C., Chance, K., de Graaf, M., Hakkarainen, J., Hassinen, S., Ialongo, I., Kleipool, Q., Krotkov, N., Li, C., Lamsal, L., Newman, P., Nowlan, C., Suleiman, R., Tilstra, L. G., Torres, O., Wang, H., and Wargan, K.: The Ozone Monitoring Instrument: overview of 14 years in space, *Atmos. Chem. Phys.*, 18, 5699–5745, <https://doi.org/10.5194/acp-18-5699-2018>, 2018.
- Lin, J.-T., Martin, R. V., Boersma, K. F., Sneep, M., Stammes, P., Spurr, R., Wang, P., Van Roozendaal, M., Clémer, K., and Irie, H.: Retrieving tropospheric nitrogen dioxide from the Ozone Monitoring Instrument: effects of aerosols, surface reflectance anisotropy, and vertical profile of nitrogen dioxide, *Atmos. Chem. Phys.*, 14, 1441–1461, <https://doi.org/10.5194/acp-14-1441-2014>, 2014.
- Lin, J.-T., Liu, M.-Y., Xin, J.-Y., Boersma, K. F., Spurr, R., Martin, R., and Zhang, Q.: Influence of aerosols and surface reflectance on satellite NO₂ retrieval: seasonal and spatial characteristics and implications for NO_x emission constraints, *Atmos. Chem. Phys.*, 15, 11 217–11 241, <https://doi.org/10.5194/acp-15-11217-2015>, 2015.
- Liu, M., Lin, J., Boersma, K. F., Pinardi, G., Wang, Y., Chimot, J., Wagner, T., Xie, P., Eskes, H., Van Roozendaal, M., Hendrick, F., Wang, P., Wang, T., Yan, Y., Chen, L., and Ni, R.: Improved aerosol correction for OMI tropospheric NO₂ retrieval over East Asia: constraint from CALIOP aerosol vertical profile, *Atmos. Meas. Tech.*, 12, 1–21, <https://doi.org/10.5194/amt-12-1-2019>, 2019.
- Lorente, A., Boersma, K. F., Yu, H., Dörner, S., Hilboll, A., Richter, A., Liu, M., Lamsal, L. N., Barkley, M., De Smedt, I., Van Roozendaal, M., Wang, Y., Wagner, T., Beirle, S., Lin, J.-T., Krotkov, N., Stammes, P., Wang, P., Eskes, H. J., and Krol, M.: Structural uncertainty in air mass factor calculation for NO₂ and HCHO satellite retrievals, *Atmos. Meas. Tech.*, 10, 759–782, <https://doi.org/10.5194/amt-10-759-2017>, 2017.
- Martin, R. V., Chance, K., Jacob, D. J., Kurosu, T. P., Spurr, R. J. D., Bucsela, E., Gleason, J. F., Palmer, P. I., Bey, I., Fiore, A. M., Li, Q., Yantosca, R. M., and Koelemeijer, R. B. A.: An improved retrieval of tropospheric nitrogen dioxide from GOME, *J. Geophys. Res. - Atmos.*, 107, <https://doi.org/10.1029/2001JD001027>, 2002.
- Martin, R. V., Jacob, D. J., Chance, K., Kurosu, T. P., Palmer, P. I., and Evans, M. J.: Global inventory of nitrogen oxide emissions constrained by space-based observations of NO₂ columns, *J. Geophys. Res. - Atmos.*, 108, D17, <https://doi.org/10.1029/2003JD003453>, 2003.
- Nakajima, T. and Tanaka, M.: Algorithms for radiative intensity calculations in moderately thick atmospheres using a truncation approximation, *J. Quant. Spectrosc. Radiat. Transfer*, 40, 51–69, 1988.
- Palmer, P. I., Jacob, D. J., Chance, K., Martin, R. V., Spurr, R. J. D., Kurosu, T. P., Bey, I., Yantosca, R., Fiore, A., and Li, Q.: Air mass factor formulation for spectroscopic measurements from satellites: Application to formaldehyde retrievals from the Global Ozone Monitoring Experiment, *J. Geophys. Res. - Atmos.*, 106, 14 539–14 550, <https://doi.org/10.1029/2000JD900772>, 2001.
- Platt, U. and Stutz, J.: *Differential Absorption Spectroscopy: Principles and Applications*, Springer, Berlin, 2008.
- Qin, W., Fasnacht, Z., Haffner, D., Vasilkov, A., Joiner, J., Krotkov, N., Fisher, B., and Spurr, R.: A geometry-dependent surface Lambertian-equivalent reflectivity product for UV-Vis retrievals – Part 1: Evaluation over land surfaces using measurements from OMI at 466 nm, *Atmos. Meas. Tech.*, 12, 3997–4017, <https://doi.org/10.5194/amt-12-3997-2019>, 2019.
- Randles, C. A., da Silva, A. M., Buchard, V., Colarco, P. R., Darmenov, A., Govindaraju, R., Smirnov, A., Holben, B., Ferrare, R., Hair, J., Shinzuka, Y., and Flynn, C. J.: The MERRA-2 Aerosol Reanalysis, 1980 Onward. Part I: System Description and Data Assimilation Evaluation, *J. Clim.*, 30, 6823–6850, <https://doi.org/10.1175/JCLI-D-16-0609.1>, 2017.
- Spurr, R. J.: VLIDORT: A linearized pseudo-spherical vector discrete ordinate radiative transfer code for forward model and retrieval studies in multilayer multiple scattering media, *J. Quant Spect. Rad. Trans.*, 102, 316–342, <https://doi.org/10.1016/j.jqsrt.2006.05.005>, 2006.

- Stammes, P., Sneep, M., de Haan, J. F., Veefkind, J. P., Wang, P., and Levelt, P. F.: Effective cloud fractions from the Ozone Monitoring Instrument: Theoretical framework and validation, *J. Geophys. Res. - Atmos.*, 113, <https://doi.org/10.1029/2007JD008820>, 2008.
- Thalman, R. and Volkamer, R.: Temperature dependent absorption cross-sections of O₂—O₂ collision pairs between 340 and 630 nm and at atmospherically relevant pressure, *Phys. Chem. Chem. Phys.*, 15, 15 371–15 381, <https://doi.org/10.1039/C3CP50968K>, 2013.
- 555 van Geffen, J., Eskes, H., Boersma, K., Maasackers, J., and Veefkind, J.: TROPOMI ATBD of the total and tropospheric NO₂ data products, S5P-KNMI-L2-0005-RP, <https://sentinel.esa.int/documents/247904/2476257/Sentinel-5P-TROPOMI-ATBD-NO2-data-products>, last access 27 August 2019, 2019.
- Vasilkov, A., Qin, W., Krotkov, N., Lamsal, L., Spurr, R., Haffner, D., Joiner, J., Yang, E.-S., and Marchenko, S.: Accounting for the effects of surface BRDF on satellite cloud and trace-gas retrievals: a new approach based on geometry-dependent Lambertian equivalent reflectivity applied to OMI algorithms, *Atmos. Meas. Tech.*, 10, 333–349, <https://doi.org/10.5194/amt-10-333-2017>, 2017.
- 560 Vasilkov, A., Yang, E.-S., Marchenko, S., Qin, W., Lamsal, L., Joiner, J., Krotkov, N., Haffner, D., Bhartia, P. K., and Spurr, R.: A cloud algorithm based on the O₂-O₂ 477 nm absorption band featuring an advanced spectral fitting method and the use of surface geometry-dependent Lambertian-equivalent reflectivity, *Atmos. Meas. Tech.*, 11, 4093–4107, <https://doi.org/10.5194/amt-11-4093-2018>, 2018.
- Veefkind, J., Aben, I., McMullan, K., Förster, H., de Vries, J., Otter, G., Claas, J., Eskes, H., de Haan, J., Kleipool, Q., van Weele, M., Hasekamp, O., Hoogeveen, R., Landgraf, J., Snel, R., Tol, P., Ingmann, P., Voors, R., Kruizinga, B., Vink, R., Visser, H., and Levelt, P.: TROPOMI on the ESA Sentinel-5 Precursor: A GMES mission for global observations of the atmospheric composition for climate, air quality and ozone layer applications, *Rem. Sens. Environ.*, 120, 70 – 83, <https://doi.org/10.1016/j.rse.2011.09.027>, 2012.
- Veefkind, J. P., de Haan, J. F., Brinksma, E. J., Kroon, M., and Levelt, P. F.: Total ozone from the ozone monitoring instrument (OMI) using the DOAS technique, *IEEE Trans. Geosci. Rem. Sens.*, 44, 1239–1244, <https://doi.org/10.1109/TGRS.2006.871204>, 2006.
- 570 Veefkind, J. P., de Haan, J. F., Sneep, M., and Levelt, P. F.: Improvements to the OMI O₂–O₂ operational cloud algorithm and comparisons with ground-based radar–lidar observations, *Atmos. Meas. Tech.*, 9, 6035–6049, <https://doi.org/10.5194/amt-9-6035-2016>, 2016.
- Zhang, W., Deng, S., Luo, T., Wu, Y., Liu, N., Li, X., Huang, Y., and Zhu, W.: New global view of above-cloud absorbing aerosol distribution based on CALIPSO measurements, *Remote Sens.*, 11, 2396, <https://doi.org/10.3390/rs11202396>, 2019.